DECLARATION

I hereby declare that this dissertation, which I submit for the qualification of

Master of Technology in Chemistry

To the Vaal University of Technology, Department of Chemistry, apart from the recognized assistance of my supervisors, is my own work and has not previously submitted to any other institution before for a research diploma or degree.

_____ on this _____ day of _____

Candidate

_____ on this _____ day of _____

Supervisor

_____ on this _____ day of _____

Co-supervisor

DEDICATION

I dedicate this work to my wife Lebohang, my mother Maphalatse, my late father, Lesley Tefo and my two loving kids Mahlatse and Tshegofatso.

ACKNOWLEDGEMENTS

I wish to sincerely acknowledge the people and organizations listed below for their valuable contribution towards the success of this project:

- Dr S.S. Manzini and Dr E.D. Dikio (my supervisors) for the moral and technical support.
- Dr S.S. Manzini of SASOL Technology, Research and Development, for help with Mössbauer Spectroscopy analyses.
- Dr P.J Mohlala of SASOL Technology, Research and Development, for assisting with Windows Microsoft 2007 for my write up.
- Bongani Xaba and Alisa Govender of SASOL Technology, Research and Development, for help with SEM and TEM analyses.
- Pule Mokhetho of SASOL Technology, Research and Development, for help with SEM and TEM sample preparation.
- Siyanda Lubhelwana of SASOL Technology, Research and Development, for help with XRD analyses.
- Jeanette Ngubane of SASOL Technology, Research and Development for help with ball milling instrument.
- SASOL TECHNOLOGY, R&D, Sasolburg for the financial support.

- The Vaal University of Technology for the academic support.

- Special thanks are due to my wife, kids, sister and parent for their support during the period of my study. May ALLAH reward you for all you have done.

- Finally I wish to thank ALLAH who has made it possible for me to come this far. ALLAH AKBAR

PRESENTATION

The work presented in this dissertation has already been presented in conferences as shown below.

1. Moloto L.H., Manzini S.S., Dikio E.D., *Reduction of hematite induced by graphite during mechanical alloying. Poster presentation,* CATSA 2009 conference, Cape Town, Rawsonville (Western Cape). 8-11 November 2009.

2. Moloto L.H., Manzini S.S., Dikio E.D., *Reduction of iron oxides induced by graphite during reactive milling.* Oral presentation, Botswana. 15th Symposium of Chemistry Graduate Students of the Universities of Botswana, Botswana, Gaborone. North West and Vaal University of Technology 2010. Moloto L.H., Manzini S.S., Dikio E.D., 29 July 2010.

ABSTRACT

Many oxidic iron compounds—iron oxides; oxy-hydroxides and hydroxides—not only play an important role in a variety of disciplines but also serve as a model system of reduction and catalytic reactions. There are more than 16 identifiable oxidic iron compounds. The reduction of these

compounds has been investigated for centuries. Despite this, the reduction behavior of the oxides is not fully understood as yet.

To date the reduction mechanism is still plagued with uncertainties and conflicting theories, partly due to the complex nature of these oxides and intermediates formed during the reduction. Thermodynamically, the reduction of iron oxide occurs in steps. For example, during the reduction of hematite (a-Fe_2O_3) magnetite (Fe_3O_4) is first formed followed by non-stoichiometric wüstite (Fe1-yO) and lastly metallic iron (a-Fe). The rate of transformation depends on the reduction conditions. Further, this reduction is accompanied by changes in the crystal structure.

The reduction behavior of iron oxides using graphite under ball-milling conditions was investigated using Planetary mono mill (Fritsch Pulverisette 6), Mössbauer Spectroscopy (MS), X-ray Diffraction (XRD), Scanning electron microscopy (SEM) and Transmission Electron Microscopy (TEM).

It was found that hematite transformed into magnetite, Wüstite and or cementite depending on the milling conditions. The study shows that by increasing the milling time, the rotational speed and / or the ball to powder ratio, the extent of the conversion of hematite to its reduction products increased. Further investigations are required for the elucidation of the reduction mechanism. The reaction og magnetite and graphite at different milling conditions lead to the formation of Fe^{2+} and Fe^{3+} species, the former increasing at the expense of Fe_3O_4. Fe_3O_4 completely disappeared after a BPR of 50:1 and beyond. The Fe^{2+} species was confirmed to be due to FeO using XRD analysis.

HRSEM images Fe_2O_3 using scanning electron microscopy prior to and after milling at different times showed significant changes while the milling period was increased, HRSEM images showed that the once well defined hematite particles took ill-defined shapes and also became smaller in size, which was a results of the milling action that induced reaction between the two powders to form magnetite. EDX spectra at different milling times also confirmed formation of magnetite. EDX elemental analysis and quantification confirmed the elemental composition of starting material consisting mainly of iron.

Similarly, HRSEM images of Fe_3O_4 using Scanning electron microscopy (SEM) prior to and after milling at different BPR showed significant changes when the milling period was increased. EDX spectra at different milling times also confirmed formation of partial FeO and EDX elemental analysis and quantification confirmed the elemental composition of starting material consisting mainly of iron than Fe_2O_3.

TEM images of both Fe_2O_3 and Fe_3O_4 particles at different milling conditions displayed observable particle damages as a function of milling period.The once well - defined particles (Fe_2O_3 and Fe_3O_4) successively took ill – defined shapes, possibly accompanied by crystallite size reduction.

MAS showed that the reactive milling of α- Fe_2O_3 and C resulted in reduction to Fe_3O_4 , FeO and or cementite depending on the milling conditions etc Time, milling speed and BPR variation which influenced the reduction. The study shows that by increasing the milling time, the rotational speed and / or the ball to powder ratio, the extent of the conversion of hematite to its reduction products increased.

XRD study investigations even though were unable to detect spm species (Fe^{2+} and Fe^{3+}) which has smaller crystallites below detection limits ,the variation in time showed an increment in the magnetite peaks accompanied by recession of hematite and graphite peaks as the milling time was increased which relates to the MAS observation.XRD also corroborated the data obtained from MAS that showed that the main constituent was magnetite and further evidence in support of the reduction of hematite to magnetite under reactive milling was obtained using XRD .

Overall, the work demonstrated selective reduction of Fe_2O_3 to Fe_3O_4 and Fe_3O_4 to FeO by fine tuning the milling conditions. It is envisaged that the reduction of FeO to Fe and possible carburization to Fe_xC could also be achieved.

TABLE OF CONTENTS

LIST OF FIGURES

LIST OF TABLES

LIST OF ABBREVIATIONS

Fe_2O_3	Hematite
Fe_3O_4	Magnetite
HRSEM	High Resolution Scanning Electron Microscopy
EDX	Electron Diffraction X-ray
BPR	Ball to Powder Ratio
TEM	Transmission Electron Microscopy
SEM	Scanning Electron Microscopy
FeO	Wustite
XRD	X-ray Diffraction
MAS	Mössbauer Absorption Spectroscopy
MSDS	Materials Safety Data Sheet
AU-Pd	Gold –Palladium

BSD	Backscatter Detector
GIF	Gatan Image Filter
HRTEM	High Resolution Transmission Electron Microscopy
Fe	Iron
CO	Carbon monoxide
C	Carbon
CO_2	Carbon Dioxide
BSE	Backscatter Electron

CHAPTER ONE

1 INTRODUCTION

1.1 Background

Many oxidic iron compounds—iron oxides, oxide-hydroxides and hydroxides—not only play an important role in a variety of disciplines and also serve as a model system of reduction and catalytic reactions [1]. There are more than 16 identifiable oxidic ion compounds. The reduction of these compounds has been investigated for centuries. For example, the reaction of iron ore has been a subject of research and discussion for many years, but to date it is still plagued with uncertainties and conflicting theories [2]. Reduction of iron oxides, uncertainties arise because of the complex nature of these oxides.

Thermodynamically, reduction of iron oxide occurs in steps: of all the iron oxides, hematite is the richest naturally occurring form because it is thermodynamically the most stable iron oxide. During the reduction of hematite (Fe_2O_3), magnetite (Fe_3O_4), non-stoichiometric wustite ($Fe_{1-y}O$) and metallic iron are formed, depending on the reduction conditions. The reduction of hematite to magnetite, wustite and metallic iron is accompanied by changes in the crystal structure [2].

Reduction studies on powdered oxides are typically made using a fluidized bed reactors or by exposing stationary samples to a flow of reducing gas. The rate at which reduction occurs is limited by the mass velocity of the gas. Sintering of the reduced particles frequently occurs, and in fluidized beds, this interferes with fluidization and changes the reaction conditions.

Direct reduction of iron oxides by solid carbon, particularly in heated bed reactors, has also been reported. The carbon source could be coke, graphite, coal, char, deposited carbon and activated carbon. It is thought that the reaction proceeds through gaseous intermediates as shown in equations. (1-3) below rather than being a genuine solid-solid reaction. It is thought that the reaction between the two solid phases (iron oxide and carbon) begins only at points of contact between the carbon and the particles of iron oxide. As soon as metallic iron appears as an intermediate phase between the other two phases contact is disrupted and further reduction can only be effected by the diffusion of gaseous CO produced as an intermediate [2].

$$Fe_xO_{Y(s)} + C_{(s)} \leftrightarrows Fe_xO_{y-1(S)} + CO_{(g)}, \quad (1)$$

$$Fe_xO_{Y(s)} + CO_{(g)} \leftrightarrows Fe_xO_{y-1(S)} + CO_{(g)}, \quad (2)$$

$$CO_{2\,(g)} + C_{(s)} = 2CO_{(g)}, \quad (3)$$

where x = 1, 2 or 3 and y = 1, 3 or 4.

The aim of this project is to investigate the reduction behaviour of iron oxides, using carbon as a reductant. The mechanical alloying (MA) process (also known as ball milling) will be used to induce reaction between the reactants. The assumption to be tested is whether a similar reduction mechanism as described above (see Eqs. (1 – 3) will also apply during ball milling processes.

1.2 Justification

Mechanical alloying (also known as ball milling) is a well established method to induce solid state reactions. For example, it has been shown that iron carbide species (hexagonal carbide ε'-$Fe_{2.2}C$, cementite θ-Fe_3C and Eckström-Adcock iron carbide, Fe_7C_3) can be formed (which is a form of oxidation) by ball milling of metallic iron with activated carbon at various stages of the milling process [3]. In contrast, the reaction of hematite with activated carbon was found to result in the reduction of the former to magnetite. Another publication suggests that the reduction of hematite should form wustite [4]. Furthermore, the reaction of magnetite with activated carbon produced no effect (i.e. no form of redox reaction). The contrasting results warrant further investigations on these systems.

Possible explanations regarding the different reduction behaviours of hematite and magnetite follow below. It could well be that the grain sizes of (and possibly, crystallite sizes) of hematite and magnetite were very different (grain sizes affect the rate of reduction of metal oxides). It is also equally possible that the reactions conditions employed differed. Another possible explanation emanates from the thermodynamics properties of the two oxides; it could be that the activation barrier for the reduction of magnetite to metallic iron or ferrous iron is rather large, requiring larger amount of energy to overcome a seemingly large activation barrier towards the formation of metallic iron. The reasons why wustite rather than magnetite forms under certain reduction conditions has not been fully explained as yet.

The results of the ball milling process in terms of the phases formed and their structural properties will be monitored using Mössbauer spectroscopy in the absorption mode and X-ray diffraction. The morphology and surface structures will be monitored using electron microscopy techniques.

1.3 PURPOSE OF THE STUDY

To investigate the solid state reaction of hematite and carbon (graphite, activated carbon) using mechanical alloying. This is to check whether magnetite and/or wustite form as intermediates during the reduction reaction as reported by different authors. The study will also look at the reduction behaviour of magnetite using carbon.

1.4 Objectives

The objective of the study is four fold

1. Verify the intermediate phase formed during the solid state of hematite and carbon using carbon mechanical alloying.
2. Study the reduction behaviours of magnetite using carbon under mechanical alloying
3. If metallic iron is formed during the reactions proposed above, its carburisation behaviour will also be investigated.

1.5 Methodology

The following actions will be taken to ensure that the above-mentioned goals are met:

- Characterize iron oxides, and carbon and products before and after mechanical alloying.
- Monitor the phase, morphology and structural properties using characterization methods like X-ray Diffraction (XRD), Mössbauer Absorption Spectroscopy (MAS), electron microscopy (transmission and scanning modes).
- Investigate mechanical alloying features like ball-to powder ratio and milling time to optimize the formation of the intended product.

1.6 Outline of the dissertation

Below is an outline of this dissertation

Chapter 1 (Introduction): this chapter gives an insight into the research work that will was carried out and its importance. Also presented in this chapter is the problem statement, the justification and the objectives of the study.

Chapter 2 (Literature review): in this chapter, a review of literature pertaining to reduction of iron oxides and their phase changes, behavior related to problem statement are presented.

Chapter 3 (Methodology): All analytical methods and experimental procedures that were used in this research project are discussed in details in this chapter.

Chapter 4 (Results and discussion): Results obtained from this study will be presented in this chapter, together with an interpretation of the results.

Chapter 5 (Conclusions): Based on the results obtained with respect to the initial objectives and hypothesis, conclusions are drawn and highlighted in this last and final chapter.

Selected spectral data appear in the **Appendix section**.

CHAPTER TWO

2 LITERATURE REVIEW

2.1 Introduction

Reduction of iron oxides is one of the most investigated topics, Due to the importance of iron and steel in current and future technologies [5].Iron compounds serve as industrial catalysts, e.g. Fe catalysts have been in use for more than 60 years in Fischer-Tropsch (FT) processes [6]. In Fe-FT, the iron oxide is first reduced to α-Fe and then carbided to form the FT active iron carbide phase.

The synthesis and development of the new alloy by mechanical means has been is existence for more than four decades. Milling consists of grinding through impact, compression and attrition. The strain, shear, thermal and kinetic energy transforms all the solids involved from one phase or compound into another through solid state reaction .The process can be performed in different gas pressure, temperature and in dry or wet (different dispersing agents) conditions [7].

Effect of grinding on the properties on the substances was first studied during the last decade of the 18^{th} century from that time; extensive research was carried out in the field of solid state mechanochemistry, which lead to accumulation of knowledge in the field [8]. Mechanical activation played an important role in mineral dressing and extractive metallurgy [23, 24, 26].

Studies showed that mechanochemistry processes could be used to induced a wide range of solid-solid and chemical reactions, this reactions studies were displacement types reaction in metal oxide which were reduced by more reactive reductants [25,26].

2.1 Mechanical Alloying and Milling

During mechanical alloying repeated welding and fracturing of powder particles increases the area of contact between the reactant due to the reduction in the particle size, which allows fresh surface to come into contact repeatedly. This allows the reaction to proceed without the necessity for diffusion through the product layer, and reactions occur at low temperatures [8].

The different methods or processes were developed through mechanical alloying methods [9]:

1. Mechanical Alloying (MA)
2. Mechanical activated annealing (M2A)
3. Double Mechanical alloying (dMA)
4. Mechanical Milling (MM)
5. Reaction Milling (RM)
6. Cromilling (CM)
7. Rod Milling (RD)
8. Oxidation-Attrition Milling-Reduction (OMR)

2.1.1 Mechanical Alloying

Mechanical alloying begins by blending individual powder constituents, which have a diameter ranging from 1 to 500µm. The powder blend, depending on the desired alloy to be processed, contained one or more ductile metal components **(Figure 1).** The starting metal can be almost any form including powder made during metal refining, or powder prepared from crushed stock.

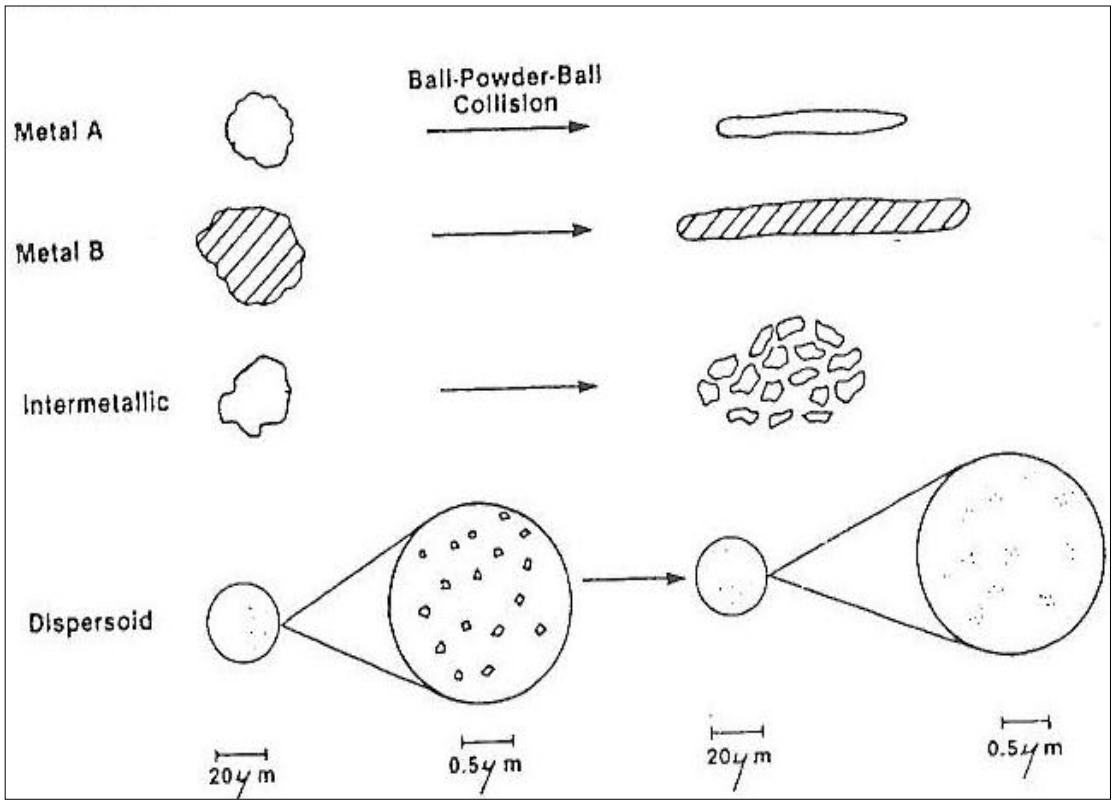

Figure 2-1: Representative constituents of starting powders used in mechanical alloying.

Ball-powder-ball collision occur when the metal particles being flattened overlap, atomically clean metal interfaces are brought into intimate contact, forming cold welds and building up layered composite powder particle consisting of various combination of the starting ingredients, **(Figure 1.2)** [10].

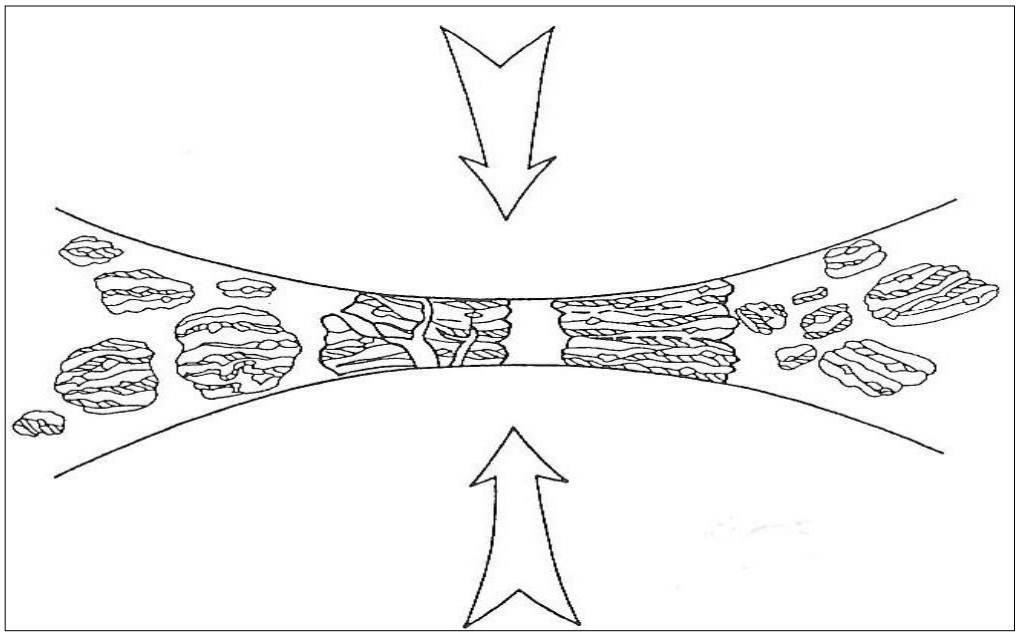

Figure 2-2: Ball –powder-ball collision of powder mixture during mechanical milling.

MA process involves optimization of a number of process variables to achieve the desired product phase, microstructure, and properties. Some of the important process variables that have an important effect on the final constitution of the milled powder are as follows [9]:

- Type of mill
- Milling container
- Milling energy/speed
- Grinding medium
- Milling time
- All-to-powder weight ratio (BPR)
- Extent of vial filling
- Milling atmosphere
- Process control agent
- Temperature of milling

2.1.2 Type of Mill

Different types of mills are available for MA/MM; these mills differ in their capacity, speed of operation, capacity to control the operation by varying the temperature of milling and the extent of

minimizing contamination of milled powders. Depending on the type of powder, quantity of powder to be milled, a suitable mill can be chosen. Most commonly used mills are SPEX shaker [Figure 2 – 5], Fritsch Pulverisette planetary ball mills [Figure 2-3] or attritors [Figure 2-6]. The degree of contamination, amount of the amorphous phase formed, crystallisation temperature, and the activation energy for crystallization of the amorphous phase depend on the type of mill used [9].

Types of mills commonly used:

2.1.2.1 Fritsch Pulverisette planetary ball mills

Planetary ball mill owes its name to the planet-like movement of its vials, they are arranged on a rotating disk, and a special drive mechanism causes them to rotate around their own axes. The centrifugal force produced by the vials rotating around their own axes and that produced by the rotating support disk both act on the vial contents, consisting of the material to be ground and the grinding balls and few hundred grams of powder can be milled at the same time [9].

Figure 2-3: Fritsch Pulverisette planetary ball mill

Since the vials and the supporting disk rotate in opposite directions, the centrifugal forces alternately act in like and opposite directions. This cause the grinding balls to run down the inside wall of the vial causing the friction effect, followed by the material being ground and the grinding

balls lifting off and travelling freely through the inner chamber of the vial and colliding with the opposing wall- impact effect **(Figure 2-4).**

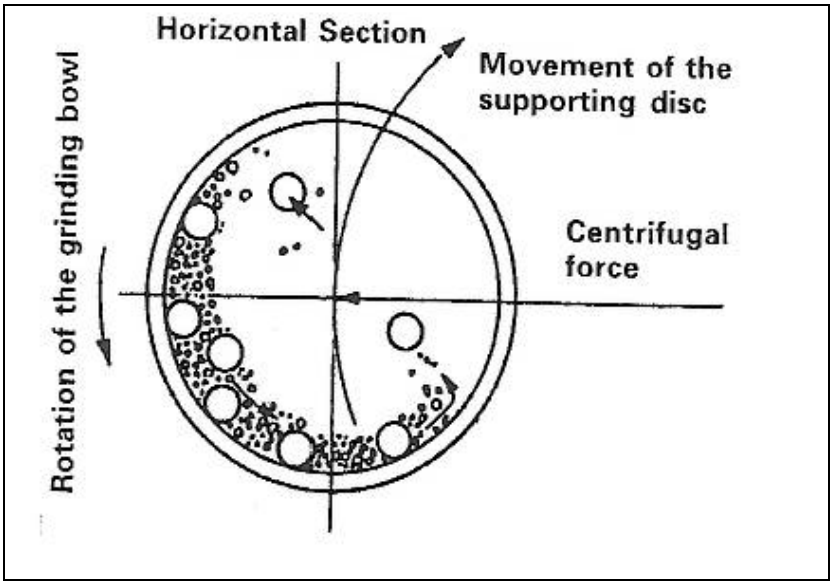

Figure 2-4: ball motion inside the planetary ball mill

The grinding balls in the planetary mills acquire much higher impact energy than with simple gravity mills. The impact energy acquired depends on the speed of the planetary mill and can reach about 20 times the earth's acceleration, as the speed is reduced, grinding balls lose impact energy, and when the energy is sufficiently low no grinding is involved; only mixing occurs in the sample, the disk and the vial rotation speeds could be controlled with the modern version [9].

The linear velocity of the balls in this type is higher than that in the SPEX mills, while the frequency of impacts is much less than in the SPEX mills [see figure 2-5].

2.1.2.2 SPEX Shaker Mills

Figure 2-5: SPEX 8000 mixer mill

2.1.2.3 Attritor

Figure 2-6: Model SD-1 Laboratory Attritor

2.1.3 Milling Container

The milling container (grinding vessel, vial, jar, and bowl) is an important component of a ball-milling due to the impact of the grinding medium on the inner walls of the container some material can be dislodged and be incorporated into the powder. This can contaminate the powder and alter the chemistry of the milled powder [9].

2.1.4 Milling Energy/Speed

The faster the mill rotates the higher will be the energy input into the powder, this is caused by the kinetic energy of the grinding medium imparted to the powder being milled. For the conventional ball mill, increasing the speed of rotation increase the speed with which the balls move. At high speeds the temperature of the vial may reach a high value, this may cause diffusion to promote homogenization and alloying in the powder [9].

Note however that an increase in temperature overly accelerates the transformation processes resulting in the decomposition of the supersaturated solid solutions or other metastable phases formed during milling. The other disadvantage of increased milling speed is the excessive wear of the milling tools, which could also lead to increased powder contamination [9].

2.1.5 Grinding Medium

The material of the grinding medium is an important variable. The higher the density of the grinding medium, the more kinetic energy it acquires during milling and this can be transferred to the powder. The size of the grinding medium has an influence on the milling efficiency; larger size of the grinding medium is useful since the larger weight of the balls transfers more impact energy to the powder particles. Therefore the final constitution of the powder is dependent on the size of the grinding medium used for milling [9].

2.1.6 Milling Time

Time is chosen to achieve a steady state between fracturing and cold welding of powder particles to facilitate alloying. The times required vary depending on the type of mill used, mill settings, intensity of milling, BPR, and temperature of milling.

2.1.7 Ball – To- Powder Ratio (BPR)

The BPR has a significant effect on time required to achieve a particular phase in the powder being milled. The higher the BPR, the shorter is the time required, and faster refinement of the crystalline size, but the amount of powder synthesized is low. Similarly lower BPR increases the amount of powder produced but the time required to reach the crystalline size is longer [9].

2.1.8 Extent of Filling the Vial

Alloying among the powder particles occurs mainly due to impact forces exerted on them, it is necessary that there be enough space for the balls and the powder particles to move around freely in the milling container. The extent of filling the vial with the powder and balls is important. If the quantity of the balls and the powder are very small, then the production rate is very low. If the quantities of the balls + powder are very large, then there is not enough space for the balls to move around so that the energy of the impact is less, resulting in alloying not occurring and if it does taking long time [9].

2.1.9 Milling Atmosphere

MA process is normally conducted under vacuum or an inert atmosphere to prevent/minimize oxidation and contamination of the milled powder. Major effect of the milling atmosphere is on the nature and extent of contamination of the powder [9].

2.1.10 Process Control Agents (PCA)

A PCA (lubricant or surfactant) is added to the powder mixture during milling to reduce the effect of excessive cold welding. PCA can be solid, liquid, or gaseous; they are mostly, organic compounds, which act as surface-active agent. They adsorb on the surface of the powder particles and minimize cold welding among powder particles and inhibiting agglomeration. They do so by lowering the surface tension of the solid material [9].

2.1.11 Temperature of Milling

Temperature of milling helps in deciding the constitution of the milled powder. Diffusion processes are involved in the formation of alloy phases, irrespective of whether the final product phase is a solid solution, intermetallic, nanostructure, or an amorphous phase, it is expected that temperature of milling will have a significant effect in any alloy system [9].

A powder processing technique that allows production of homogeneous materials starting from blended elemental powder mixtures [10]. MA is a generic term for processing of metal powders in high – energy ball mills, depending on the state of the starting powder mix and processing steps involved. MA describes the process when mixtures of powders (of different metals or alloys/compounds) are milled together to produce a solid solution and material transfer is involved to obtain a homogeneous alloy [9].

Mechanical alloying can be created without melting, by violently deforming mixtures of different powders, **Figure 2-7**. Inert oxides can be used by this technique, introduced equally into

microstructure. The dispersion – strengthened alloyed powders are consolidated using hot-isostatic pressing and extrusion, to produce a solid with a very fine grain structure. Heat treatment then induces recrystallisation, into a fine, equiaxed set of grains [6].

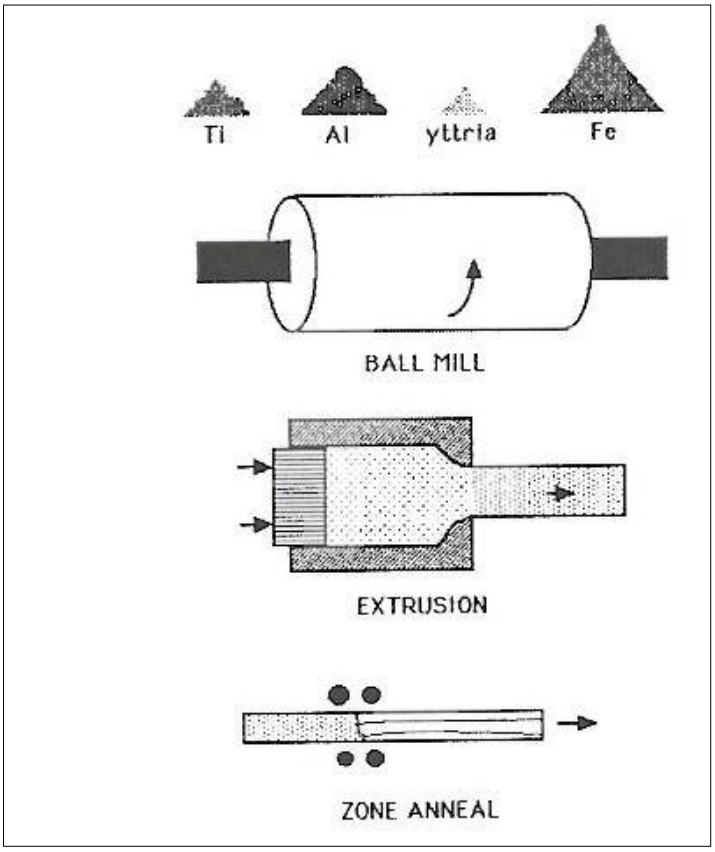

Figure 2-7: Manufacture of mechanically alloyed metal for engineering application.

Fundamental processing in mechanical alloying to produce metal powders with controlled microstructures is the repeated welding, fragmenting, and rewelding of a mixture of powders in a dry, highly energetic ball charge. This occurs under conditions in which the rates of welding and fracturing are balanced and average powder particle size remains relatively coarse [10]. In this machine the ball charge is activated by impellers radiating from a rotating vertical central shift, **Figure 2-8.**

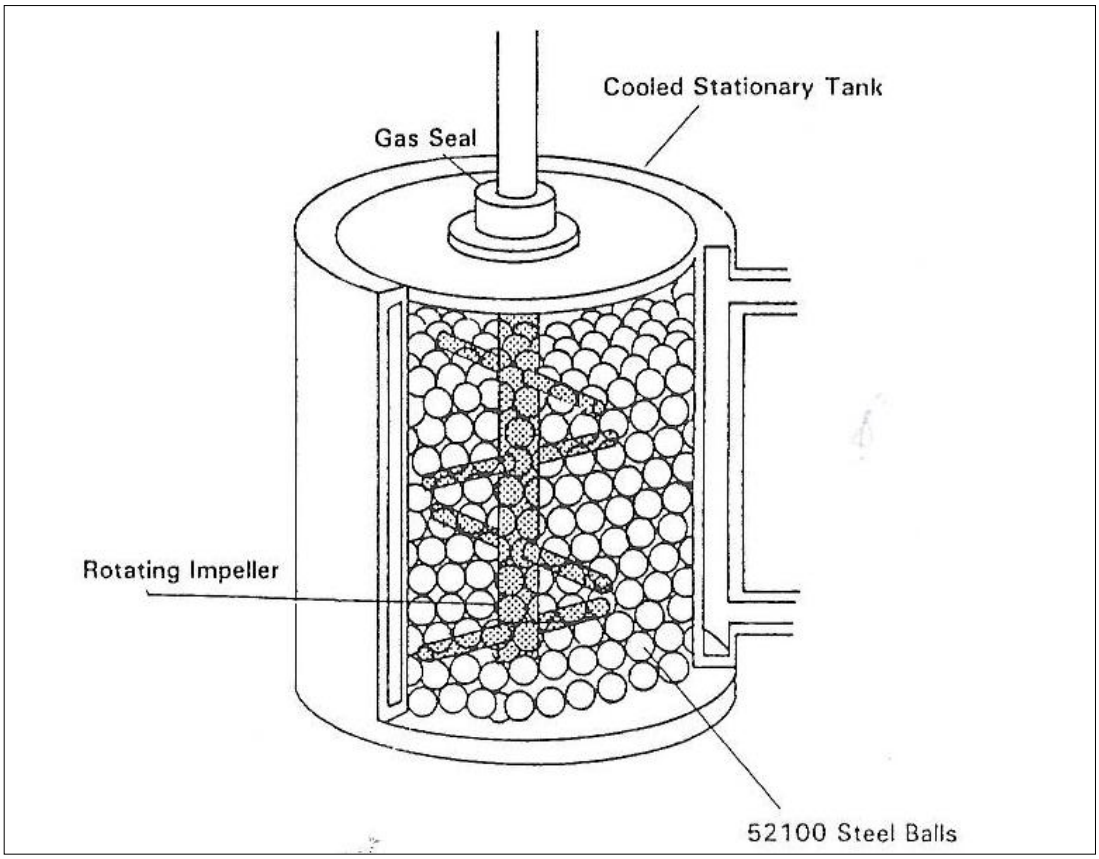

Figure 2-8: Highly energetic type ball mill used for mechanical alloying.

Conventional ball mills that rotate around a central horizontal axis can be used for mechanical alloying as long they are of sufficient size (>1m in diameter) and are operated under highly energetic conditions. It requires operating the mill just below the critical speed that would spin the balls to the internal walls of the mill and reducing the weight of the powder charge relative to the ball charge. The ball charges consist of 52100-bearing steel grinding balls; this balls fabrication from alloys may be used to avoid minor contamination through ball wear [10].

2.1.12 Mechanically Activated Annealing

It is a process that combines short MA duration with a low temperature isothermal annealing. This combination was found to be effective in producing refractory material.

2.1.13 Double Mechanical Alloying

The process involves two stages of milling. During the first stage, the constituent elemental powder sizes are refined and equally distributed as an intimate mixture. The mixture is then subjected to heat treatment at high- temperature during which intermetallic phases are formed. During the

second stage, the heat treated powder is milled again to refine powder size of the intermetallic phases and reduce the grain size of the surrounding substance [9].

2.1.14 Mechanical Milling

When powders of uniform composition, such as pure metals, intermetallics, or prealloyed powders, are milled in a high-energy ball mill, and material transfer is not required for homogenization, also if pure metal or an intermetallic is processed only to reduce particle size and increase the surface areas, then material transfer is not involved. Advantage of MM over MA is that powders are already alloyed and only a reduction in particle size has to be induced mechanically, the time required for processing is short [9].

2.1.15 Reaction Milling

It is the MA process accompanied by a solid-state reaction and the powder is milled without the aid of any process control agent to produce fine dispersions of oxides and carbides [9].This is the mechanical milling process of choice for this project.

2.1.16 Cryomilling

Milling operations are carried out at cryogenic (very low) temperatures and milling of material is done in a cryogenic medium such as liquid nitrogen. During this process the vessel is cooled by a continuous flow of the cryogen through the water cooled jacket of the mill. After completion of the milling run, the powder is removed from the mill in the form of slurry and transferred to dry in a glove box containing argon [9].

2.1.17 Rod Milling

This process was developed in Japan (1989) to reduce powder contamination during processing stages; the grinding medium is in the form of rods rather than spherical balls [9].

2.1.18 Oxidation – Attrition Milling-Reduction

Commercially available powders are oxidized at appropriate temperatures to produce brittle oxide powders, which are then subjected to attrition milling to obtain nanoscale oxide powders. The nanoscale oxide powders are subsequently reduced to metallic powders with nanometer grain size. This method is important to produce nanocrystalline powders of ductile metals and materials [9].

2.2 Fe Oxide phase transformation by ball milling

Phase transformation of simple iron oxides during mechanical activation has been extensively studied over the last two decades [11]. Phase transformation of iron oxides was first reported by Uehara, where he showed the transformation induced in iron oxides after 80 hour milling in polar and nonpolar mediums [12]. Investigating the structure of dry milled hematite powder under nitrogen atmosphere, where they observed nanocrystalline magnetite [13].

Introduction of hematite and water(wet milling) into vial and milled in a vertical low energy device, and controlled the gas atmosphere inside the vial by pressure valve and used low vacuum during milling operations, where total transformation of α-Fe_2O_3 to Fe_3O_4 was observed [14].

These finding were also observed and confirmed by other researchers , where they reported that the mechanism of hematite to magnetite transformation in a sealed vial was bond breaking during high energy ball milling followed by release of oxygen from the vial [15,16,17,18].

Transformation reaction was induced to ball milling of iron oxides, α-Fe_2O_3 in both air and oxygen atmospheres under closed milling condition which has been studied for detailed characterization of the microstructure of all the evaluated phases on milling up to 10 hours. The results revealed transformation of α-Fe_2O_3 to Fe_3O_4 and finally to FeO occurring in both air and oxygen atmospheres, the reaction speed was slower in oxygen environment. The reaction was controlled by oxygen partial pressure, which decreases on continuing milling. Critical oxygen partial pressure was reached at 3 - 4 hours of milling, when Fe_3O_4 attains maximum saturation. Prolonged milling (7-10 h) resulted in further reduction of oxygen partial pressure, resulting in complete transformation of α-Fe_2O_3 and Fe_3O_4 to FeO, except that the transformation reaction was slow in oxygen [19].

Direct transformation from hematite to maghemite during energy ball milling was observed when hematite α-Fe_2O_3 powder was milled with a dispersant liquid (ethanol) at different times using planetary ball mill equipped with steel vial. The results (HRTEM; X-ray diffraction and mössbauer spectrometry) revealed the milling conditions favoured the direct transformation [20].

2.2.1 Effect of mechanical milling on phase changes of the powder

Phase transformation and structure changes of the blended powder due to milling was studied based on the XRD patterns of unmilled and milled powder mixture under different condition.

XRD patterns of unmilled and 150 hour milled powder shown in **Figure 2-9** were done in low-energy conventional ball milling with powder-to-ball weight ratio of 1:6, vial was opened frequently for sampling, being assumed that the partial pressure of gases surrounding remained fairly constant Fe_2O_3 to Fe_3O_4. Magnetite phase was not observed in the patterns, this is based on the findings of Zdujić [18].The peak intensity of graphite was decreased due to the changing of the crystalline structure and decreased the crystalline size of graphite [18].

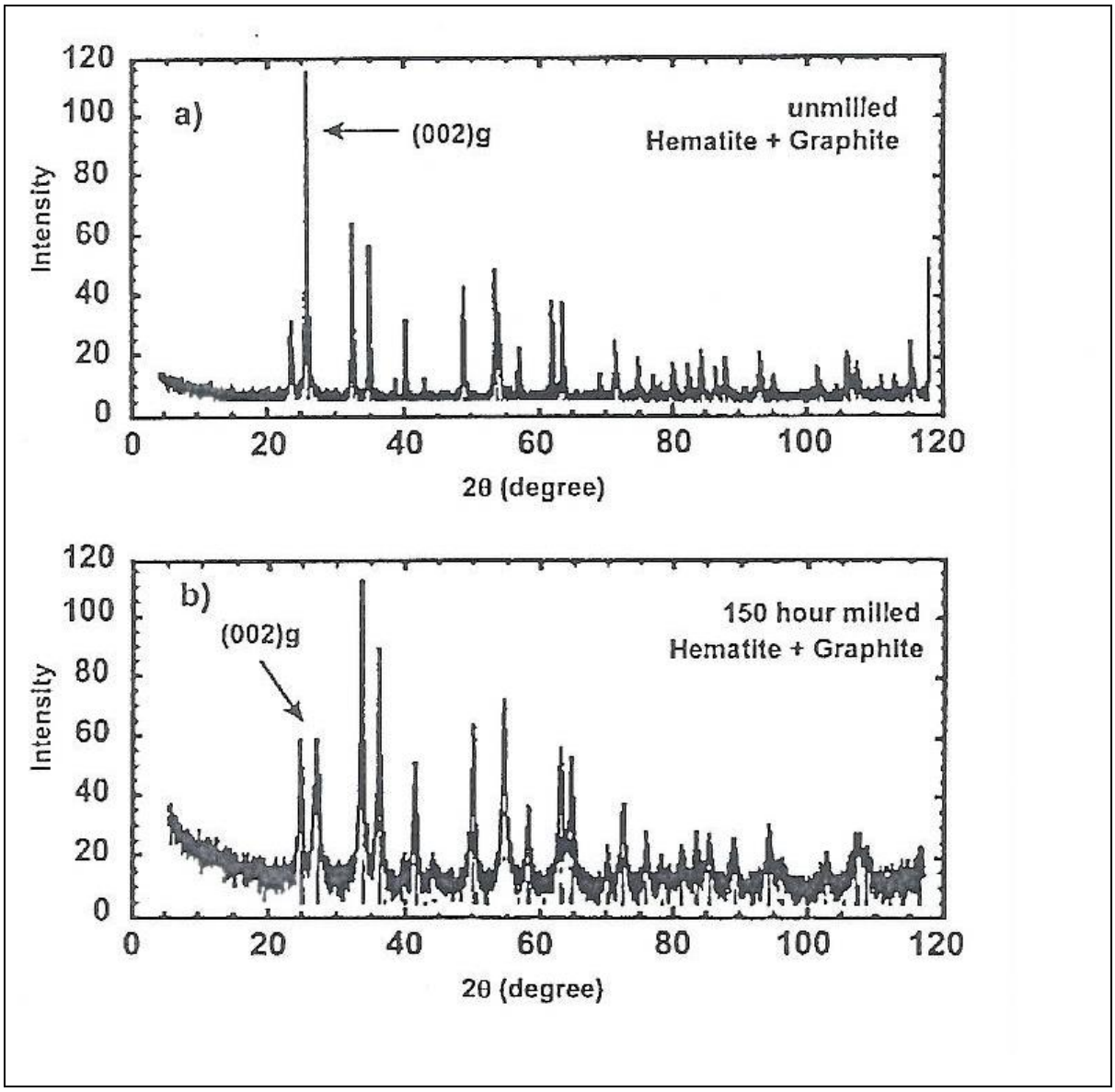

Figure 2-9: XRD pattern of unmilled and 150-hour milled powder mixture of hematite and graphite in low-energy conventional ball mill (Fe_2O_3: C = 1:3)

Figure 2.10 showed the effect of milling atmosphere on the XRD pattern of high-energy milled blend, the powder blend was milled in a large- scale planetary ball mill for 48 hours with powder-to-ball weight ratio of 1:5 [18]

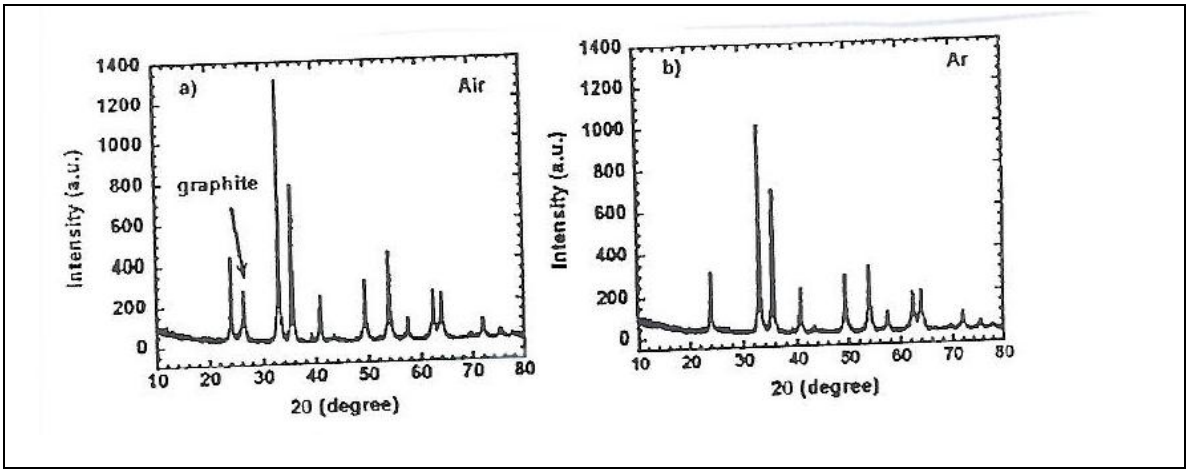

Figure 2-10: XRD pattern of 48-hour milled powder mixture of hematite and graphite in large-scale planetary ball mill under (a) air and (b) argon atmosphere (Fe_2O_3: C = 1:3.3)

Based on the observation the peak of graphite in the powder milled in argon atmosphere disappeared. In case of milling in air atmosphere part of the energy applied on the graphite during milling has contributed in oxidation of graphite while in the milling under argon atmosphere all the energy would contribute in the change of crystalline structure of graphite into amorphous structure and graphite peak disappears during milling of powder blend under argon [18].

2.2.2 Reduction of Fe Oxide + Carbon by ball milling

The reduction of iron oxides, from hematite to iron, is a complex of interrelated steps, with many new observations and still some unexplained questions [21]. the first to study mechanical reduction of hematite with carbon during ball milling, where they proved that the solid state reduction of hematite to nanocrystalline wustite resulted by milling of hematite powder in the presence of carbon, they also showed that part from wustite crystalline magnetite can be formed in the process [22].Tokumitsu observed only magnetite in the products while wustite and metallic iron were not observed in the same experiment [23].

The reductions of metal oxides are usually carried out at high temperature in suitable appropriate condition with respect to equilibrium thermodynamics, using the high activity of fresh surfaces enabling mechanically activated reduction, after ball-milling of hematite, α-Fe_2O_3 with carbon powder; hematite was reduced to magnetite [24].

The Solid state reduction of Hematite (α- Fe_2O_3) can be reduced to wűstite in room temperature by dry ball milling of hematite and carbon, in an inert atmosphere and further transformation of wustite to form magnetite, the reaction is completed by dry milling for 70h [25].

2.2.3 Effect of milling on reduction behaviour of powder blend

The recent study of the effect of mechanical milling on the reduction rate of hematite-graphite mixture by Vahdati Khaki using TG-DTA, showed that under 1100°C, the reduction mechanism was a direct reduction of iron oxide with graphite, where their peaks of each reaction curve on TG-DTA moved towards the low temperatures range and the reaction degree increased with increasing milling time [26].

The TG curves of unmilled and conventionally milled samples heated in argon atmosphere shown in **Figure 2-11**, represent three-stage endothermic reaction, which corresponds to Fe_2O_3 – Fe_3O_4, Fe_3O_4 – FeO and FeO – Fe, the second and third stages have been overlapped and the final stage of reduction has not been completed. It can be seen from the figure that the milling time made the weight loss from 1100°C to increase while the reduction temperature of various stages of reduction decreased [27].

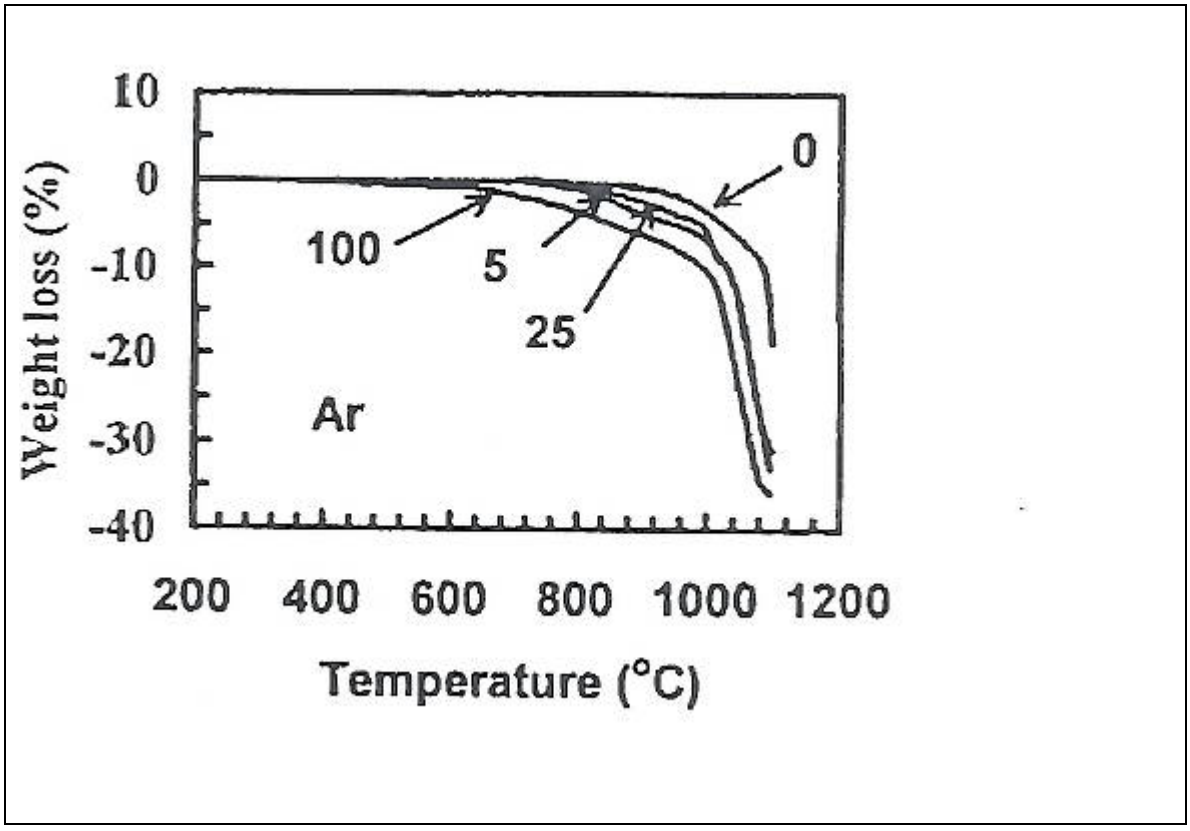

Figure 2-11: Effect of milling time at low-energy conventional ball mill on the TG curves under argon atmosphere (Fe_2O_3: C = 1:3)

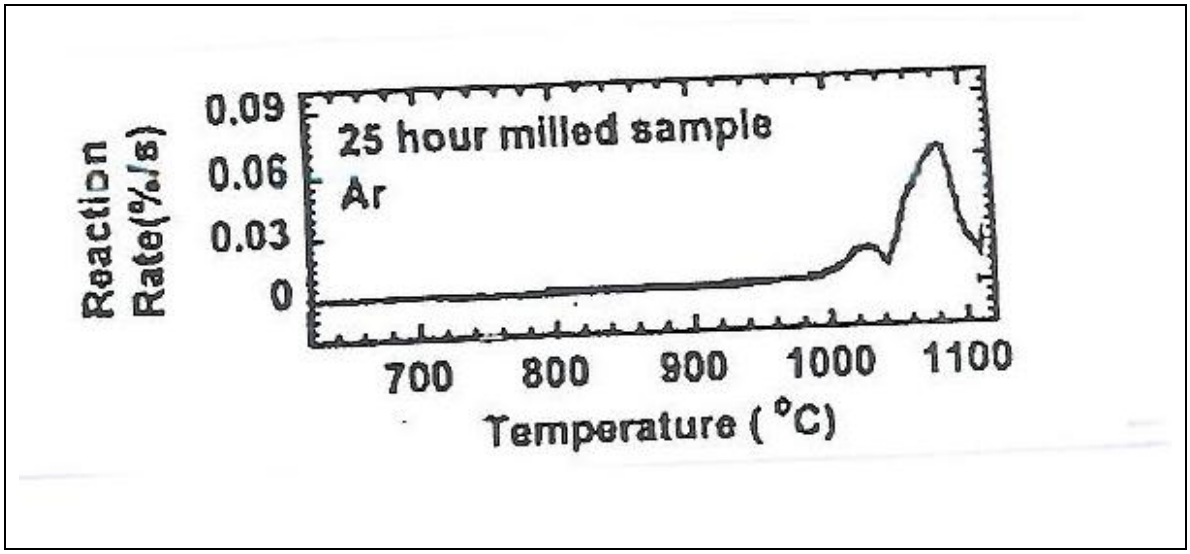

Figure 2-12: reaction rate curve from differentiation of TG curves in argon for 25-hour milled sample in low-energy conventional ball mill (Fe_2O_3: C = 1:3)

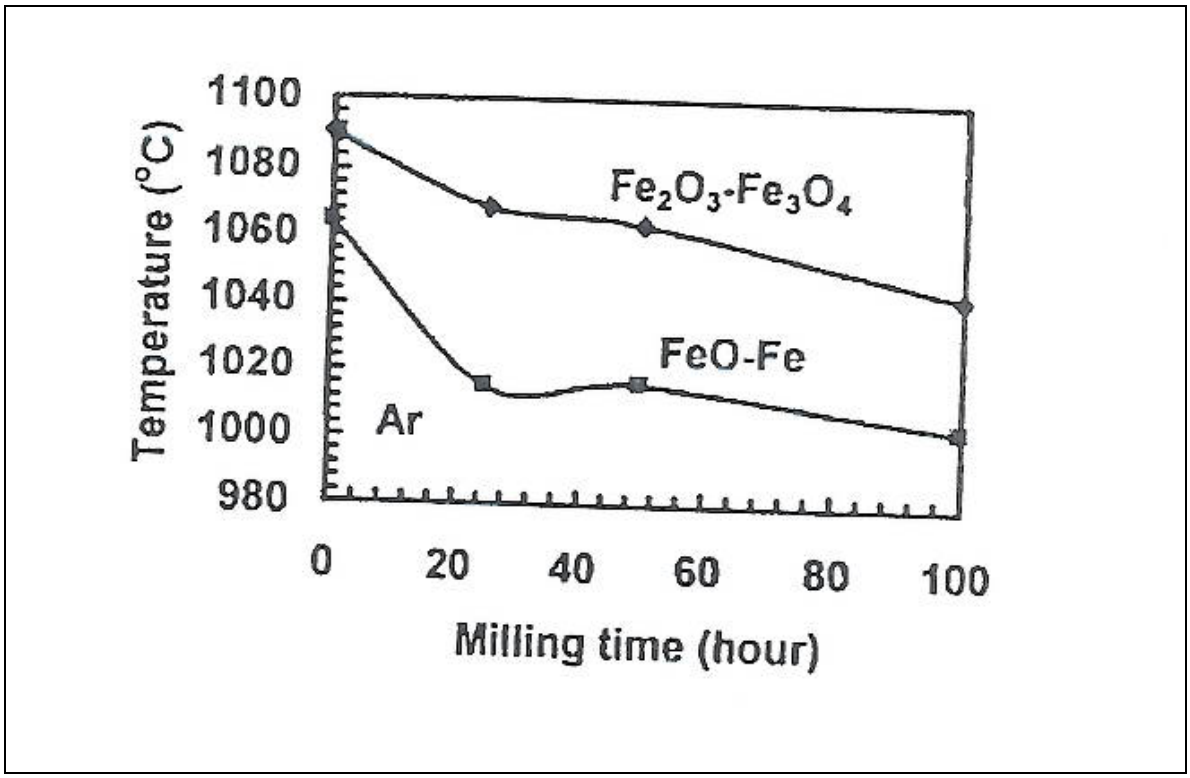

Figure 2-13: Effect of milling time at low-energy conventional ball mill on the temperature of maximum reaction rate under argon atmosphere (Fe_2O_3: C = 1:3)

The effect of milling of powder in a large- scale planetary ball mill under air atmosphere (high-energy milling) on the reduction temperature of hematite **Figure 2-14**, it was seen that the reduction temperature of the mixture is decreased drastically due to the high-energy milling and the reduction

temperature of wustite to iron reached about 750° C, where powder-to-ball weight ratio was 1:5 at rate of 10° C/min up to 1100°C, holding for 30 minutes at this temperature were cooled [27].

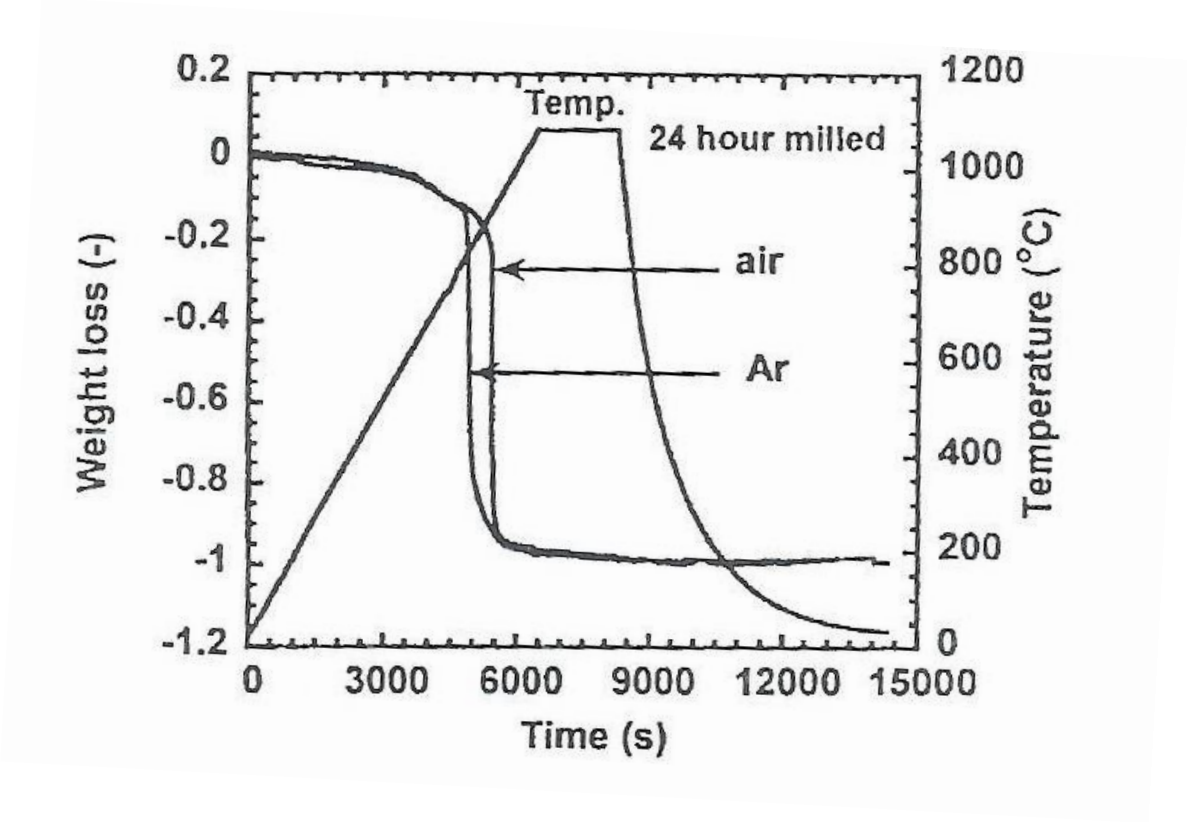

Figure 2-14: Effect of milling time in a large-scale planetary ball mill under air atmosphere on the TG curves under argon atmosphere (Fe_2O_3: C = 1:3.3)

2.3 Summary

Despite all the above studies carried out in terms of mechanical reduction of iron oxide my ball milling, there is a lack of information about reduction of mechanically activated mixtures of iron oxides. Further investigations are needed to clarify the effects of different influential parameters on the reduction behaviour of mechanically activated iron oxides.

CHAPTER THREE

3 EXPERIMENTAL METHODS

3.1 Introduction

Experimental techniques that were used in this execution of the research project are discussed in this chapter. The techniques utilized in this project have well documented protocols and were thus used as directed. All safety standards were followed to ensure safe usage of the technique. In the case where chemical reagents were used, the MSDS (materials safety data sheet) were obtained and necessary pre-cautions also taken to ensure safe usage.

3.2 Characterization Techniques

3.2.1 Planetary mono mill (Fritsch Pulverisette 6)

Planetary ball mill produces planet-like movement of its vials, which are arranged on a rotating disk, and a special drive mechanism causes them to rotate around their own axes. The centrifugal force produced by the vials rotating around their own axes and that produced by the rotating support disk both act on the vial contents, consisting of the material to be ground and the grinding balls. A few hundred grams of powder can be milled at the same time [9].

The reactive milling was performed using high planetary mono mill (Fritsch Pulverisette 6). The materials to be milled were prepared by either mixing α-Fe_2O_3 (Hematite) (Sigma-Aldrich, 99, 9 %) or Fe_3O_4 (Magnetite) (Sigma-Aldrich, 98, 0 %), with graphite (Sigma-Aldrich, < 20 µm, synthetic) in a glass vial according to a pre-determined metal oxide: graphite ratio. The oxide-carbon mixture was then placed on the outer edge of the inner vial bowl. Stainless steel balls (of sufficient number to obtain the required ball to powered ratio, PBR) were then placed at the centre of the bowl. The balls used had diameter of 15 mm. The vial was sealed under an argon atmosphere before initiating the milling process. The milling conditions are summarized in Table 3.1 and 3.2. Once the operating parameters were set, milling was initiated and the system operated unattended controlled by a pre-set program. It must be emphasized however that the instrument conducted milling for 30 minutes followed by a 30 minutes of rest to prevent excessive temperature rise. At the end of the milling period, the powder was allowed to rest for an additional 3 hours to ensure ambient condition equilibration. The vial was then opened and the powder collected for characterization. The bowl and

balls were thoroughly cleaned using soap and water and properly dried. Silica powder was then ball-milled for an hour to thoroughly clean the bowl and balls.

Table 3-1: F_2O_3/C (2:3 mole ratio) milling conditions

BPR	Time (h)	Speed (rpm)
10 20	0 5 10 15 20	100 200 300 400

Table 3-2: F_3O_4/C (1:2 mole ratio) milling conditions

BPR	Time (h)	Speed (rpm)
20 30 50 60 100	15	400
40	15	400 450 500

3.2.2 Mössbauer Spectroscopy (MS)

MAS analyses the energy levels of the nucleus with extremely high accuracy and reveals the oxidation state of the atom and how large the magnetic field is at the nucleus. The technique is also used to identify phases, and can be used to follow the kinetics of bulk reactions.

^{57}Fe Mössbauer spectra were measured on a constant acceleration spectrometer (fit for purpose built in Sasolburg using components from sources such as Wissenchaftliche electronic GMBH) in a triangular mode with a 50 mCi ^{57}Co:Rh source. Spectra for the different iron-bearing samples were obtained at room temperature and for few samples at 4.2K and external magnetic field of 10T. The spectra were fitted with Lorentzian-shaped lines to obtain the Mössbauer parameters, i.e., isomer shift (δ), quadrupole splitting (ΔE_Q), and hyperfine field (B_{hf}). Isomer shift values are reported relative to metallic iron (α-Fe).

The peak positions in a Mössbauer spectrum are described in terms of the isomer shift (δ, which arises from the difference in *s*-electron density between the source and the absorber) and quadrupole splitting (ΔE_Q, which arises from the interaction between the nuclear quadrupole moment and the electric field gradient at the nucleus), when the magnetic moment is zero. The combination of δ and ΔE_Q is sufficient to assess the valence state and coordination polyhedron surrounding each Fe atom in a structure. Results of this characterization are presented in **Chapter 4**.

3.2.3 X-ray Diffraction (XRD)

XRD is one of the oldest and most frequently applied techniques in catalyst characterisation, it is used to identify crystalline phases, sizes inside the catalyst by means of lattice structural parameters, and to obtain an indication of particle size.

X-ray powder diffractograms were collected using a Philips X-pert Pro multipurpose diffractometer equipped with the X'Celerator detector. The X-ray generator was operated at 40 kV and 40 mA producing Co Kα radiation of average wavelength 1.78897 Å. The data were collected at ambient temperature and atmospheric pressure conditions. The diffractograms were measured from 5 °2θ to 105 °2θ at a scan speed of 0.014 °2θ with step sizes 0.017 °2θ measured using an automatic divergence slit to irradiate a fixed sample length of 10 mm over a 2 hr period. Crystalline phases were identified using X'Pert HighScore Plus. Results of this characterization are presented in **Chapter 4**.

3.2.4 Scanning electron microscopy (SEM)

SEM is a technique that is used to study the surface morphology or physical nature of solids. SEM uses a beam of electrons to scan through the surface of the sample. As the surface is scanned

through, a variation in electron current which is dependent on the surface properties occurs. This variation is depicted as a map showing the surface morphology of the sample.

FEG SEM- ZEISS ULTRA 55 Scanning microscope was used in sample analyses. The instrument uses a field emission tungsten hairpin filament with a ZrO reserve, as an electron source. The milled samples were mounted on aluminium stubs using double-sided carbon tape. A thin layer of Au-Pd was sputtered onto the samples in order to make the surfaces more conductive. Viewing of the specimen was performed by mounting the samples into SEM (FEG SEM- ZEISS ULTRA 55 Scanning microscope) for higher resolution scanning electron microscopy (HRSEM) and irradiating the specimen with a beam of electrons. This was followed by proper magnification and focusing for a better viewing of the specimen's surface.

In a second preparation method, a small amount of catalyst powder was transferred into a plastic mould and mixed with resin. After a sufficient curing period the sample block was removed and the surface where the catalyst particles are situated was polished to obtain a smooth flat surface. The polishing procedure uses diamond paste with progressively smaller diamond particles. After the polishing process, a thin layer of Au-Pd was sputtered onto the sample surface in order to make the surface electrically conductive.

An EVO 50HV SEM was used. The instrument uses a tungsten filament as an electron source. Elemental mapping and BSE were performed using a Bruker XFlash SDD detector that is controlled by Bruker ESPIRIT software. Backscatter Electron (BSE) images were obtained at 25kv using BSD backscatter electron detector. Images will be shown in **Chapter 4**.

3.2.5 Transmission Electron Microscopy (TEM)

Transmission Electron Microscopy (TEM) uses transmitted and diffracted electrons; the instrument is in a sense similar to an optical microscope.Primary electron beam of high energy and high intensity passes through a condenser to produce parallel rays, which impinge on the sample, the attenuation of the beam depends on the density and the thickness, and the transmitted electrons form a two-dimentional projection of the sample mass. The dark-field image is obtained from the diffracted electron beams, which are slightly off-angle from the transmitted beam. This is followed by proper magnification and focusing for a better viewing of the specimen(s).

The sample preparation for this technique, a small amount of the milled sample was mixed with ethanol, then ultrasonicating for a few minutes in ethanol in order to further break up the particles. The suspension was left standing for a few minutes in order to settle out the larger particles.

A Phillips CM200 TEM with LaB_6 filament as electron source was used for this analysis. A few drops of this suspension were extracted using a Pasteur pipette and dropped onto a holey carbon copper TEM grid. This instrument is operated at 200KV. Digital TEM images are obtained using a Gatan Image Filter (GIF) attachment that houses a CCD camera. Images will be shown in **Chapter 4**.

CHAPTER FOUR

4 RESULTS AND DISCUSSIONS

4.1 Introduction

Results obtained from this study are presented and discussed in this chapter. These include characterization of the pure hematite, pure magnetite and graphite standards (or starting materials) using the various techniques that have been discussed in the previous chapter.

4.2 Characterization of iron oxide by MAS and XRD

Figure 4-1 shows room temperature Mössbauer absorption spectra of hematite and graphite mixture (3:1 mol equivalent) ball milled at different rotational velocities (rpm) for 20h and BPR of 20. The corresponding hyperfine parameters of all phase identified as a result of the interaction of the oxide and graphite are summarised in **Table 4-1**.

Figure 4-1a shows a spectrum of unreacted hematite (the starting material). The spectrum exhibits a sextet (6 line), with parameters δ = 0.37 mm/s, ΔE_Q = -0.21 mm/s and B_{hf} = 51.5 T that is characteristic of the iron oxide at temperature below 955 K [28].

Figure 4-1b shows the spectrum of hematite and graphite mixture (3:1 mol equivalent) ball milled at a rotational velocity of 100 rpm for 20h (when the BPR was kept constant at 20:1). The spectrum was fitted with three sextets. The first sextet had parameters that corresponded to hematite. The remaining two sextets had parameters δ = 0.28 mm/s, ΔE_Q = 0.01 mm/s, B_{hf} = 49.1 T for the A site (tetrahedral coordination); δ = 0.65 mm/s, ΔE_Q = 0.02 mm/s, B_{hf} = 46.0 T for the B site (octahedral coordination) corresponding to magnetite. You will recall that magnetite is an inverse spinel, i.e., 8 Fe^{3+} cations are in a tetrahedral coordination (A sub-lattice) with 4 O^{-2} anions, while 8 Fe^{3+} cations and 8 Fe^{2+} cations are in octahedral (B sub-lattice) with 6 O^{-2} anions [28,31]. Hence, the structural formula $Fe^{3+}[Fe^{2+}Fe^{3+}]O_4$. In typical spinels, the larger cation, like Fe^{2+} in this example, should have been in the A sub-lattice. The ratio of Fe cations on A-site and B-site as well as Fe^{3+}/Fe^{2+} ratio for a given sample provide an indication of stoichiometry. For pure magnetite Fe (A-site)/Fe (B-site) ratio is expected to be 1:2 while the Fe^{3+}/Fe^{2+} is 2:1 [32]. The amount of magnetite in this sample was rather small, yet the above mentioned ratios were nearly obeyed.

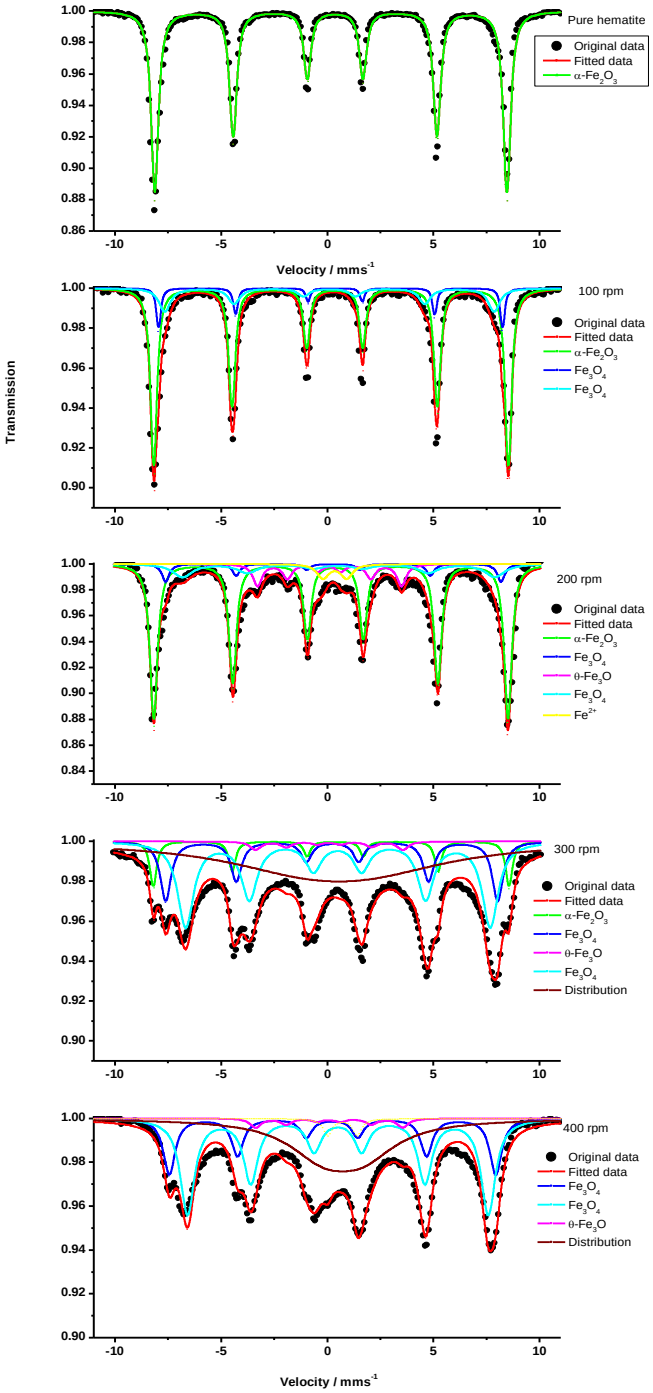

Figure 4-1: Room temperature Mössbauer absorption spectra of hematite and graphite mixture (3:1 mol equivalent) ball milled at different rotational velocities (rpm) for 20h and at a constant BPR of 20:1, showing the different identified phases that resulted from the interaction

Table 4-1: MAS parameters of the ball-milled hematite and graphite mixtures at different rotational speeds for 20 hours at a constant BPR of 20:1.

Milling speed (rpm)	**MAS parameters**			**Phases**	
	$^{\#}\ \delta$ / mms^{-1}	$^{\#}\ \Delta E_Q$ / mms^{-1}	$^{\phi}\ B_{hf}$ / T	Formula	Common Name
0	0.37	-0.21	51.5	α-F e_2O_3	Hematite
100	0.37	-0.21	51.4	α-F e_2O_3	Hematite
	0.28	0.01	49.1	Fe_3O_4	Magnetite
	0.65	0.02	46.0		
200	0.37	-0.21	51.5	α-F e_2O_3	Hematite
	0.28	-0.02	49.4		
	0.66	0.08	46.2	Fe_3O_4	Magnetite
	0.19	0.01	21.4	θ-Fe_3C	Cementite
	0.56	1.22	-	Fe^{2+}	Unresolved Fe^{2+} species
300	0.37	-0.21	51.7	α-F e_2O_3	Hematite
	0.28	-0.01	49.0	Fe_3O_4	Magnetite
	0.64	0.03	46.2		
	0.18	-0.04	21.7	θ-Fe_3C	Cementite
	0.65	1.17	-	Fe^{2+}/ Fe^{3+}	Distribution of Fe^{2+}/ Fe^{3+} species
400	0.28	0.00	49.3	Fe_3O_4	Magnetite
	0.64	0.03	45.8		
	0.18	-0.01	21.8	θ-Fe_3C	Cementite
	0.78	80	-	Fe^{2+}	Wüstite
	0.67	1.20	-	Fe^{2+}/ Fe^{3+}	Distribution of Fe^{2+}/ Fe^{3+} species

Figure 4-2 shows the X-ray diffractogram of hematite and graphite mixture (3:1 mol equivalent) ball milled at a rotational velocity of 100 rpm while the other variables (BPR = 20:1 and time = 20h) were kept constant. The diffractogram displayed sharp and intense 2θ lines that were easily assigned to their phase constituents. The peaks were assigned to hematite and graphite phases (which were the starting materials). No trace amount of magnetite was observed using XRD (unlike MAS that showed a small contribution from the iron oxide). The discrepancy was tentatively contributed to crystallite size of the newly formed magnetite to be much smaller to be detected by XRD technique.

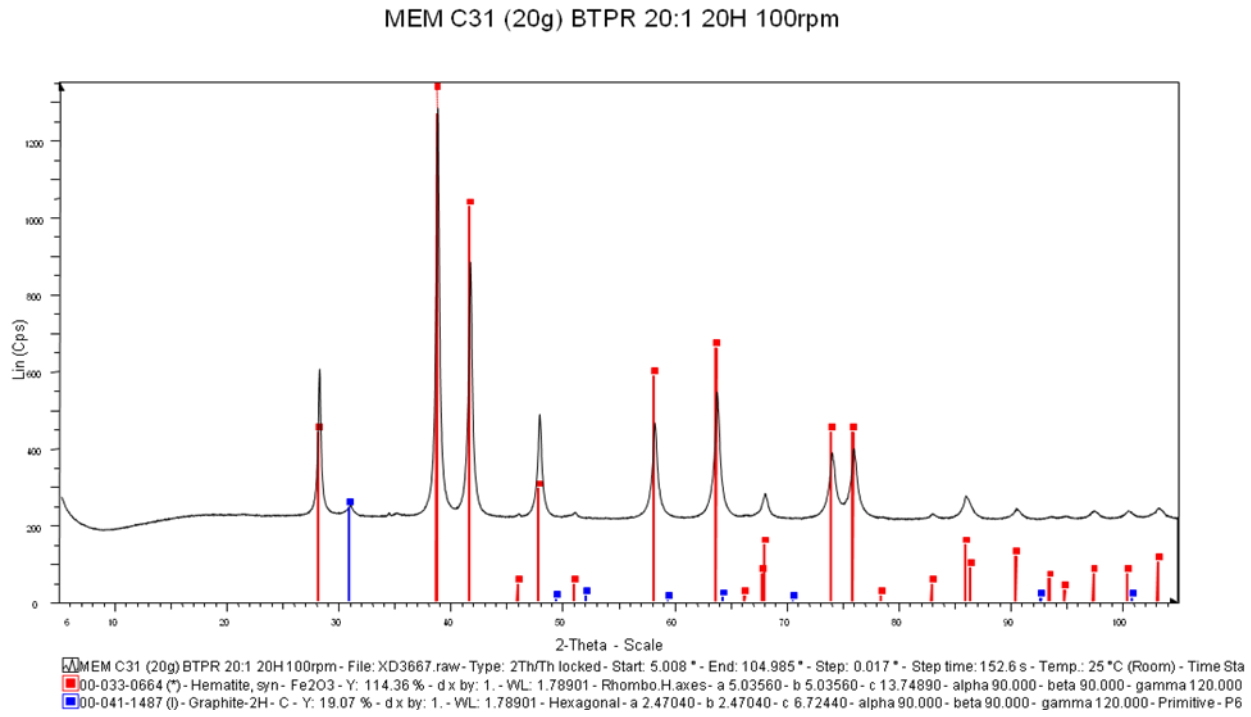

Figure 4-2: X-ray diffractogram of hematite and graphite mixture (3:1 mol equivalent) ball milled at a rotational velocity of 100 rpm, BPR of 20:1 for 20h

Figure 4-1c show the spectrum of hematite and graphite mixture (3:1 mol equivalent) ball milled at a rotational velocity of 200 rpm for 20h. The spectrum was fitted with four sextets coexisting with a qudrupole doublet (2-line). One sextet had parameters that matched those of hematite while two sextets matched those of magnetite. The fourth sextet with parameters, δ = 0.19 mm/s, ΔE_Q = 0.01 mm/s, B_{hf} = 21.4 T, was tentatively assigned to cementite (θ-Fe_3C). The presence of such iron carbide was unexpected under the experimental conditions followed and was thus thought to originate from contamination of either the bowl or balls used during ball milling. The minor quadrupole doublet with parameters, $\delta \sim 0.56$ mm/s, $\Delta E_Q \sim 1.22$ mm/s, was due to an Fe^{2+} species whose identity could not be unambiguously assigned using room temperature MAS. The use of LT-MAS could have aided in the resolution of the peak.

Figure 4-1d depicts the spectrum of hematite and graphite mixture (3:1 mol equivalent) ball milled at a rotational velocity of 300 rpm for 20h. The spectrum was fitted with 4 sextet and a distributions of doublets that simulate the quantity of unresolved Fe^{2+} and or Fe^{3+} species present in the sample. However, the four sextets were fully resolved and they corresponded to hematite (one sextet), magnetite (2 sextets) and cementite (one sextet), the parameters of which were similar to those mentioned above.

Figure 4-1e displays the spectrum of hematite and graphite mixture (3:1 mol equivalent) ball milled at a rotational velocity of 400 rpm for 20h. In addition to the sextet fitted for hematite, 2 sextets for magnetite, a sextet for cementite, a distribution was fitted to simulate probably a mixture of unresolved Fe^{2+} and or Fe^{3+} species. The contribution of the unresolved species increased significantly when the hematite and graphite mixture were milled at 400 rpm rather than 300 rpm.

Figure 4-3 depicts the X-ray diffractogram of hematite and graphite mixture (3:1 mol equivalent) ball milled at a rotational velocity of 400 rpm (while BPR = 20:1 and period = 20h). The peaks displayed were broad. Nevertheless, the 2θ lines were unambiguously assigned to hematite, magnetite and graphite phases. Both hematite and graphite peaks were much smaller (as would be expected when their contents were much smaller, also taking into account refractive indices of the constituents). The XRD results corroborated the data obtained from MAS that showed that the main constituent was magnetite. However, there was another difference between XRD and MAS in that the latter also detected small amounts of carbide. Again the size of the newly formed carbide was thought to be undetectable using XRD technique.

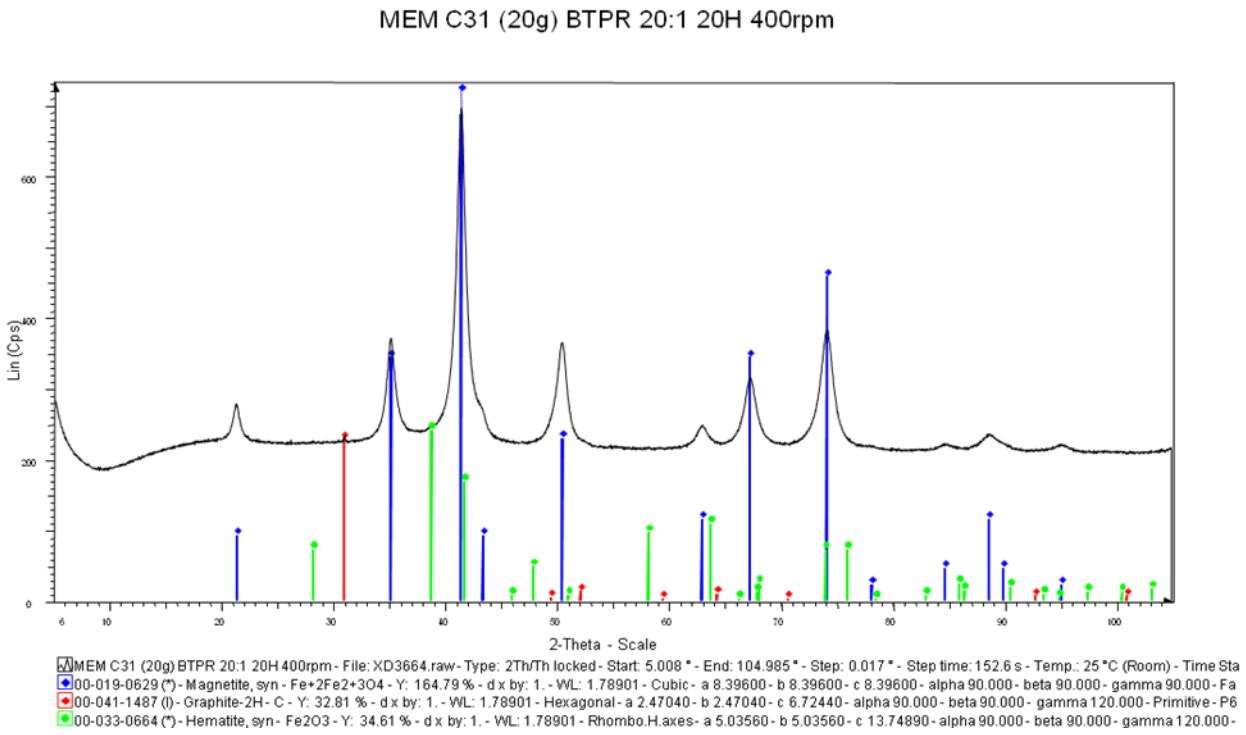

Figure 4-3: X-ray diffractogram of hematite and graphite mixture (3:1 mol equivalent) ball milled at a rotational velocity of 400 rpm (while BPR = 20:1 and period = 20h)

The interaction of hematite with graphite (3:1 mol equivalent) at different milling conditions led to the formation of magnetite and unresolved Fe^{2+} and or Fe^{3+} species. By increasing the rotational speed from 100 – 400 rpm while keeping the BPR at 20:1 and milling period at 20h, the extent of reduction of hematite increased as evidenced by the increased amount of magnetite and unresolved Fe^{2+} and or Fe^{3+} species (see Figure 4-1).

Figure 4-4 shows the amount of residual hematite after ball-milling at different rotational velocities while the milling period and BPR were kept constant at 20h and 20:1 respectively. It is evident that the amount of hematite converted to products increased with increasing milling speed. Although not exactly determined, the plot did give a hint of a near-linear relationship between hematite conversions with milling speed. Also apparent was the fact that rotation speeds exceeding 300 rpm resulted in less changes (i.e., the amount of hematite left was negligible).

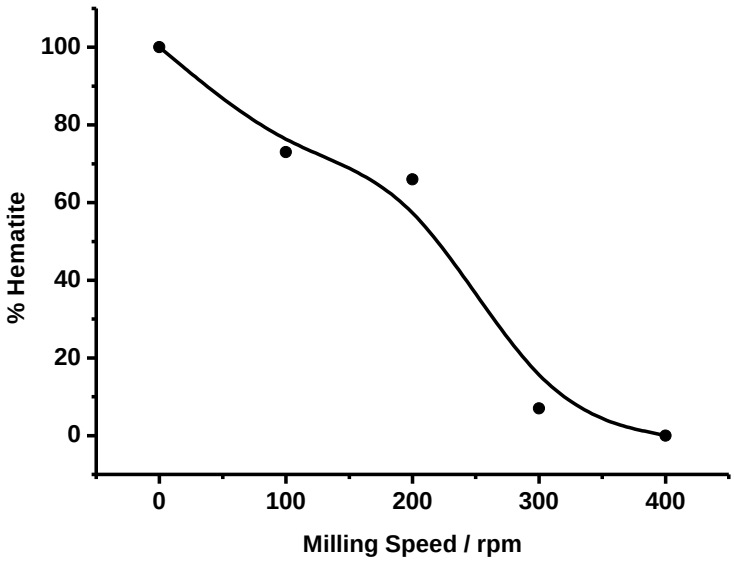

Figure 4-4: The amount of hematite detected by MAS probe as a function of milling speed (rpm) when the oxide is reduced using graphite

It was apparent that the other variables (milling speed, BPR) could also affect the reduction of hematite using graphite under reactive milling. The two variables were investigated singly starting with the milling speed variation. The phases obtained were identified and quantified using MAS. The use of XRD was restricted as it was evident that the data obtained would have been comparable to that of MAS.

The effect of milling period on the reduction of hematite with graphite was also investigated (see Figure 4-5). In this case, hematite-graphite mixture (3:1 mol equivalent) was subjected to different milling times when both BPR (20) and rotational velocity (400 rpm) were kept constant. An exponential relationship was observed such that times in excess of 10 hours were sufficient to obtain above 90% conversion of the starting material.

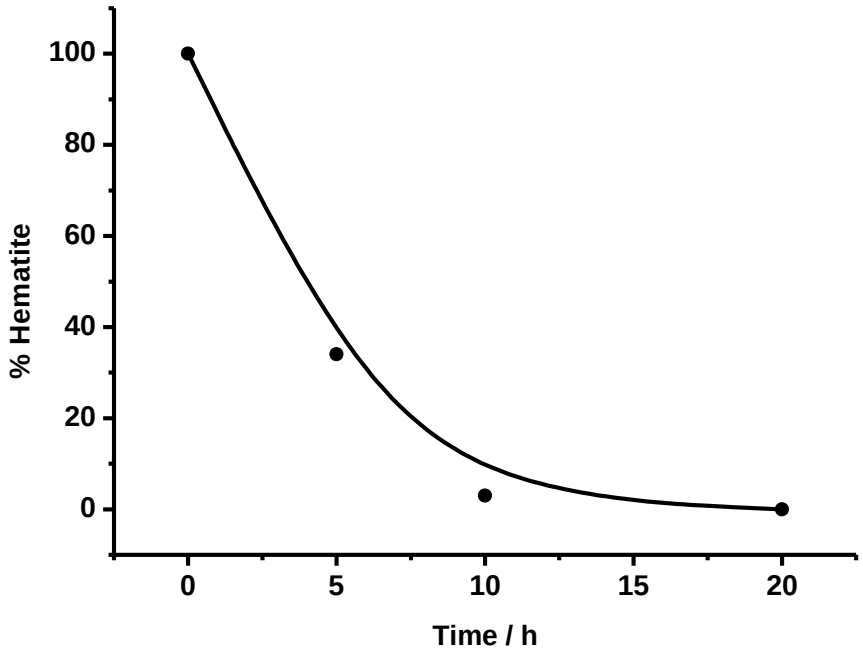

Figure 4-5: The effect of milling time on the amount of hematite left (as determined using MAS analysis) when the oxide was reacted with graphite at constant rotational speed and BPR.

Figure 4-6 graphically depicts the effect of the weight of balls to the powder (BPR) variation while milling the hematite-graphite mixture. This was achieved by milling hematite-graphite mixture (3:1 equivalent) at different BPR when both milling speed (400 rpm) and time (20h) were kept constant. The graph showed a steady increase in hematite conversion to products as the BPR was increased. BPR of more than 15 was sufficient to convert more than 90% of the starting materials.

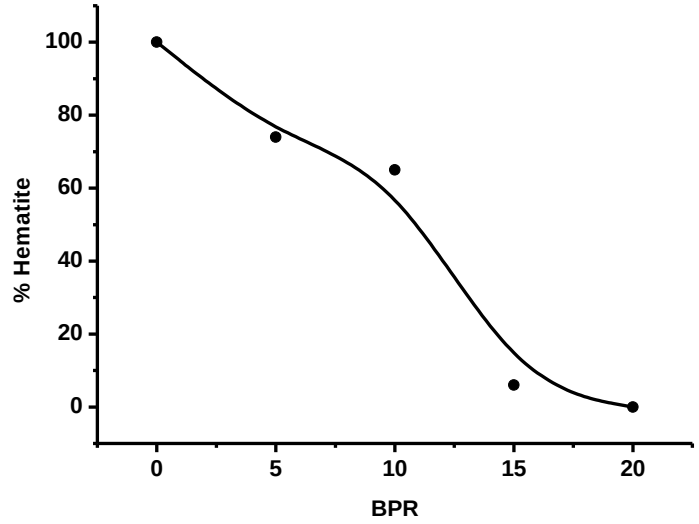

Figure 4-6: The effect of ball to powder variation (PBR) on the amount of hematite left (as determined using MAS analysis) when the oxide was reacted with graphite at constant rotational speed and period.

The interaction of hematite and graphite (3:1 mol equivalent) at different milling conditions lead to the formation of magnetite and unresolved Fe^{2+} and or Fe^{3+} species depending on the milling conditions. In some experiments, trace amounts of cementite were also detected. The iron carbide was thought not to arise from the reaction itself but as a contaminant from the bowl or balls used during the milling process. The study shows that by increasing the milling time, the rotational speed and / or the ball to powder ratio, the extent of the transformation of hematite to the above mentioned products increased. A further investigation on the reduction behaviour of magnetite was necessary for the elucidation of the reduction behaviour of hematite by graphite.

The uncertainty of the data due to the contaminations either from the milling bowl or ball prompted a change of the milling apparatus (bowl and balls). It was thought that data free of contaminants will be more appropriate for work that could be consumed by the broader scientific community. Besides, there are numerous publications that show the presence of trance amount of contaminants that speeds up or hinder certain reactions. We had to be certain that the observed reduction of hematite to magnetite was indeed as a result of the milling process in the presence of graphite rather than reaction acceleration/deceleration by the contaminant. Thus the reaction was repeated as described above but using a different milling apparatus (bowl and balls).

Figure 4-7 shows the percentage composition of the hematite and graphite mixture (3:1 mol equivalent) that was ball milled at different rotational velocities while the BPR and milling period were kept constant at 20:1 and 20h respectively. The plot shows a steady increase in the amount of magnetite and superparamagnetic (spm) species whilst the amount of hematite receded. The identity of the spm species cannot be deduced using room temperature MAS but it is speculated that they are either due to the presence of small hematite or magnetite crystallites. Most often during MAS analysis quadrupole doublets with parameters consistent with Fe^{3+} and / or Fe^{2+} are encountered and are fitted with broad lines. The broadening of the lines can be due to a superposition of several components, indicative of the distribution of crystallite size or due to the presence of small crystallites which exhibit superparamagnetic (spm) behaviour at room temperature [28]. Superparamagnetism phenomenon [29] is the collapse of the magnetically split component (sextet) into paramagnetic doublets or singlets at temperatures below the Curie temperature (magnetic ordering temperature) of the bulk material. This is caused by the fast relaxation of the magnetic vector due to thermal excitation at room temperature [30].

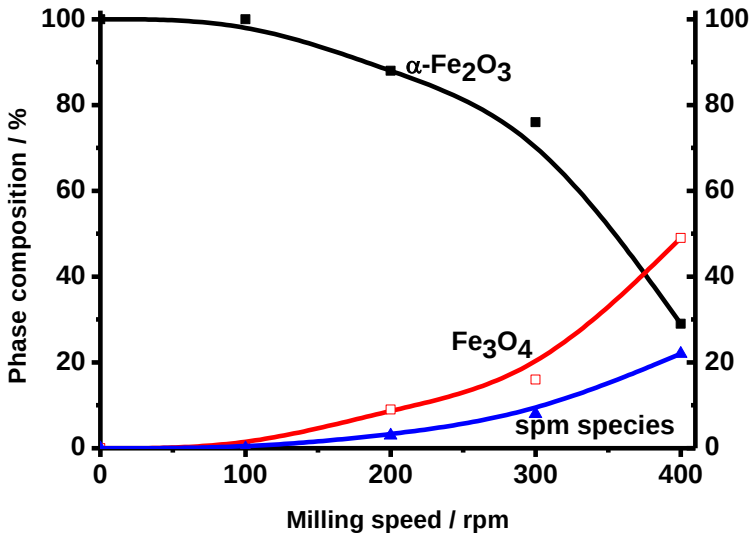

Figure 4-7: The percentage composition of the hematite and graphite mixture (3:1 mol equivalent) that was ball milled at different rotational velocities while the BPR and milling period were kept constant at 20:1 and 20h respectively, as determined using MAS.

To determine the true extent of reduction, it was necessary to quantify the amount of Fe^{2+} species in the product mixture. This was easily determined from hematite (all Fe^{3+} species), magnetite (1/3 Fe^{2+} and 2/3 Fe^{3+}) that were then combined with the spm Fe^{2+} and spm Fe^{3+} species. The total amount of Fe^{2+} divided by Fe^{3+} species was plotted as a function of rotational speed (see Figure 4-8). The plot showed exponential growth (extent of reduction).

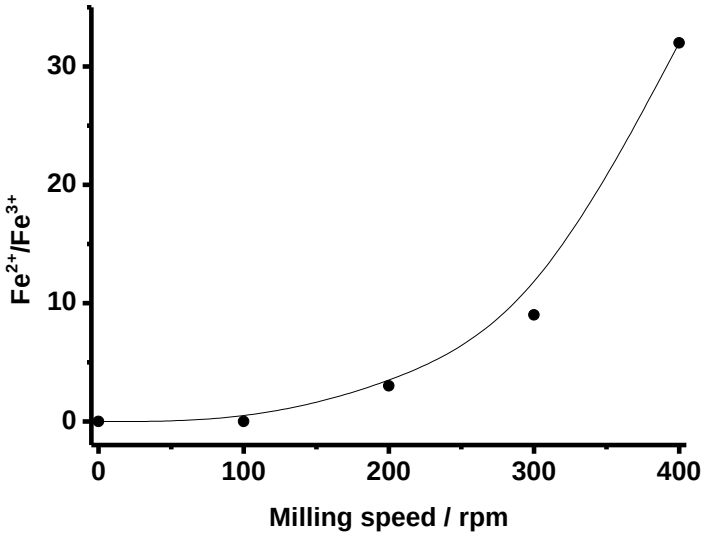

Figure 4-8: Extent of reduction (Fe^{2+}/Fe^{3+}) as a function of rotational speed when hematite and graphite (3 mol equivalent) mixture was ball milled for 20h when the BPR was kept at 20:1.

There was a need to determine, at least for one experiment, the exact compositions of the reaction mixture using LT-MAS. Due to the cost of conducting such an experiment, only one set of data was possible. In this case, the use of applied external magnetic field at low temperatures enhanced the quantification process. Figure 4-9 shows the MAS data for hematite and graphite (3 mol equivalent) mixture prepared at BPR of 20:1, milling speed of 400 rpm for a period of 20 h. The parameters are summarised in Table 2. For the sake of clarity, the spectral information is expanded below.

Figure 4-9a shows the room temperature spectra. The spectrum consists of 3 sextets superimposed on two quadrupole doublets. The outer-most sextet with parameters, δ = 0.37 mm/s, ΔE_Q = -0.21 mm/s and B_{hf} = 51.2 T was assigned to hematite. The remaining two sextets had parameters δ = 0.29 mm/s, ΔE_Q = 0.01 mm/s, B_{hf} = 48.9 T; δ = 0.62 mm/s, ΔE_Q = 0.03 mm/s, B_{hf} = 45.3 T and they were assigned to magnetite. The quadupole doublet with parameters, δ = 0.43 mm/s, ΔE_Q = 1.08 mm/s was assigned to Fe^{3+} species while the other doublet with parameters, δ = 0.99 mm/s, ΔE_Q = 1.20 mm/s was assigned to Fe^{2+} species (see Table 2).

The unresolved doublets were magnetically split at 4.2 K to either magnetite or hematite (see Figure 4-9b). The spectrum was fitted with 4 sextets. The resolution thus confirmed that indeed the Fe^{2+} and Fe^{3+} species were paramagnetic at room temperature, and the effect was due to their small crystallites, hence the resolution at lower temperatures. However, the resolutions of these species came at a small price, the broadening of the peaks at lower temperatures. This made the quantification of the two constituents a little difficult. However, the parameters that corresponded to hematite were δ = 0.48 mm/s, ΔE_Q = 0.39 mm/s and B_{hf} = 54.0 T. The remaining 3 sextets with parameters, δ = 0.51 mm/s, ΔE_Q = 0.01 mm/s, B_{hf} = 52.1 T; δ = 0.41 mm/s, ΔE_Q = 0.04 mm/s, B_{hf} = 50.4 T and δ = 0.76 mm/s, ΔE_Q = -0.57 mm/s, B_{hf} = 48.9 T were assigned to magnetite (see Table 2).

An external magnetic field of 10 T was then applied (parallel to the gamma ray) to the sample at 4.2 K in a quest to get the quantification of magnetite and hematite better. The spectrum obtained is shown in Figure 4-9c. This spectrum too was fitted with 4 sextets (one for hematite and three for magnetite). However, the line widths of the spectrum recorded at 4.2 K in applied field were slightly larger than those obtained in zero field spectrum (Figure 4.9b) and significantly larger than room temperature spectrum (Figure 4.9a). The broadening of the line widths in applied magnetic field is believed to be caused by shape anisotropy of the sample analysed [34].

The parameters for the sextet corresponding to hematite were δ = 0.49 mm/s, ΔE_Q = 0.08 mm/s and B_{hf} = 54.2 T. It is immediately apparent that both the isomer shift and the hyperfine magnetic field were unaffected by the applied external magnetic field but the quadrupole splitting dropped significantly to near zero value, suggesting a more symmetrical environment (octahedral void) where the Fe^{3+} atoms were located.

What was also significant was that the peaks corresponding to hematite were in isolation (i.e., there were hardly any interference from magnetite peaks, making its quantification much more accurate, hence the quantification of magnetite was also accurate given the binary nature of the iron oxide mixture). A close scrutiny of the hematite peaks showed that the intensities of the peaks changed compared to the sample analysed at 4.2 K without an external magnetic field. The intensities of the peaks corresponding to the Zeeman transition $\Delta m = 0$ (i.e. lines 2 and 5) increased from 2 to about 3.7. The intensities of the peaks corresponding to the Zeeman transition $\Delta m = + 1$ (peaks 1 and 6) and $\Delta m = - 1$ (peaks 3 and 4) remained unchanged at 3 and 1, respectively (see Figure 4-9c). The observed phenomenon is typical of antiferromagnetic materials where, in response to applied magnetic fields, the moments reorient themselves in such way that they all lie near the plane normal to the applied field (i.e. the atomic spins reorient perpendicular to the applied field). This is as expected for α-Fe_2O_3 which is antiferromagnetic at 4.2 K [32].

As for magnetite spectral lines (3 sextets), the outermost lines with parameters, δ = 0.38 mm/s, ΔE_Q = 0.02 mm/s and B_{hf} = 59.6 T were due to Fe^{3+} on the A sites (see Figure 4.9c and Table 4.2). The middle sextet with parameters, δ = 0.52 mm/s, ΔE_Q = -0.02 mm/s and B_{hf} = 44.1 T was due to Fe^{3+} on the B sites. The inner-most sextet with parameters δ = 0.87 mm/s, ΔE_Q = -0.59 mm/s and B_{hf} = 40.1 T was due to Fe^{2+} on the B sites.

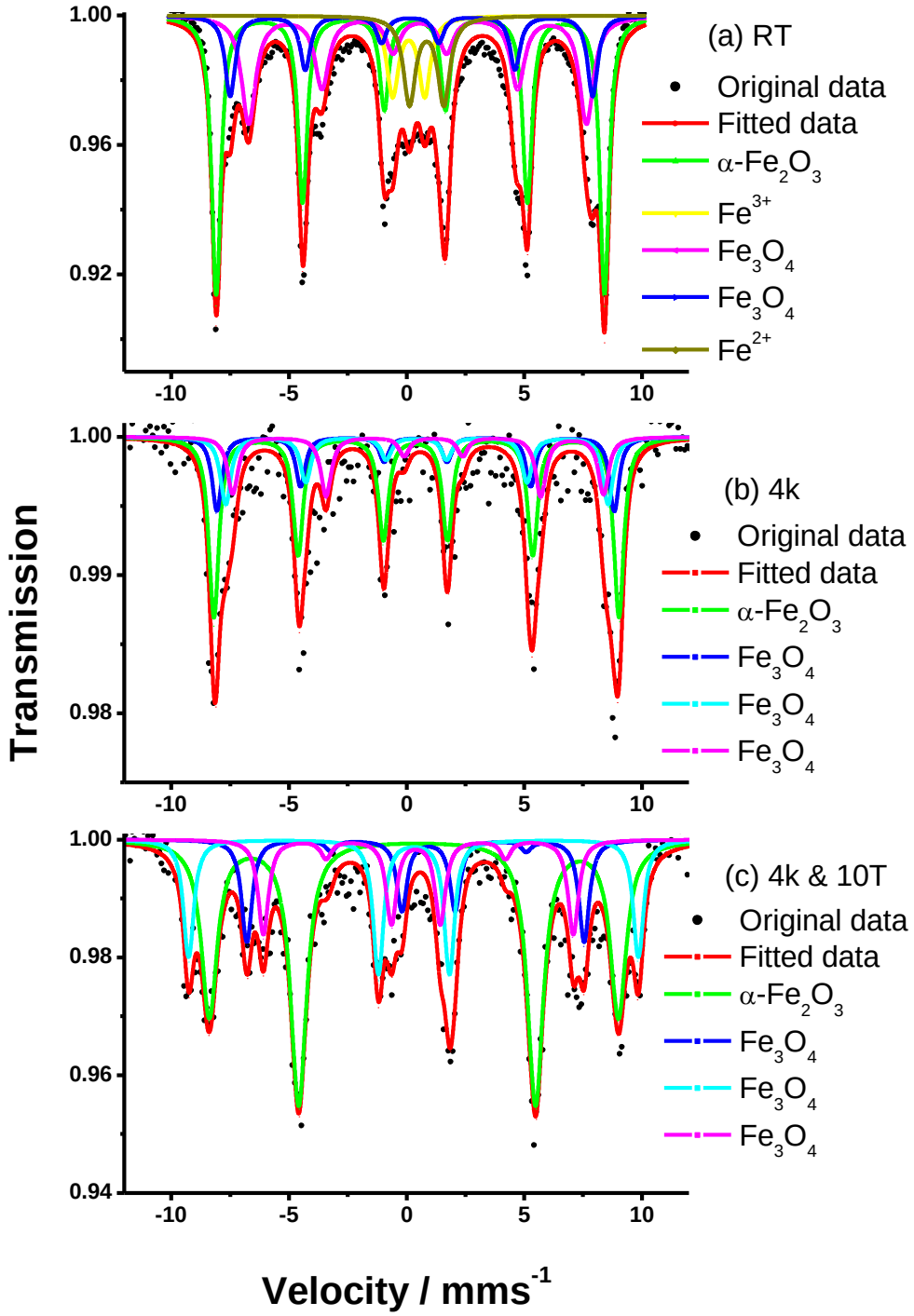

Figure 4-9: MAS spectra for sample prepared at BPR of 20, 400 rpm and 20 h of milling taken at (a) room temperature, (b) 4.2 K and (c) at 4.2 K in applied magnetic field of 10 T parallel to γ-rays.

Table 4-2: The MAS parameters for a sample of hematite and graphite (3 mol equivalent) mixture prepared at BPR of 20:1, milling speed of 400 rpm for 20 h

Sample Name	**# δ / mms^{-1}**	**# ΔE_Q / mms^{-1}**	**Φ B_{hf} / T**	**Phase**	**▪Content / %**
RT-MAS	0.37	-0.21	51.2	α -Fe_2O_3	29
	0.29	0.01	48.9	Fe_3O_4	49
	0.62	0.03	45.3		
	0.99	1.20	-	spm Fe^{2+}	12
	0.43	1.08	-	spm Fe^{3+}	10
4K	0.48	0.39	54.0	α -Fe_2O_3	33
	0.51	0.01	52.1	Fe^{3+} (Fe_3O_4)	32
	0.76	-0.57	48.9	Fe^{2+} (Fe_3O_4)	32
	0.41	0.04	50.4	Fe^{3+} (Fe_3O_4)	33
4K-10T	0.38	0.02	59.6	Fe^{3+} (Fe_3O_4)	67
	0.52	-0.02	44.1	Fe^{3+} (Fe_3O_4)	
	0.87	-0.59	40.1	Fe^{2+} (Fe_3O_4)	
	0.50	-0.08	54.0	α -Fe_2O_3	33

Figure 4-10 depicts the plot of percentage composition versus time when hematite and graphite (3 mol equivalent) mixture was ball milled at a rotational speed and BPR were kept at 20 rpm and at 20:1 respectively. The plot similarly shows a steady growth in the amounts of both magnetite and spm species whiles the amount of hematite receded with time. The true extent of reductions was also determined by plotting Fe^{2+}/Fe^{3+} versus time. The dependence of the extent of reduction on milling period was almost linear (see Figure 4-11).

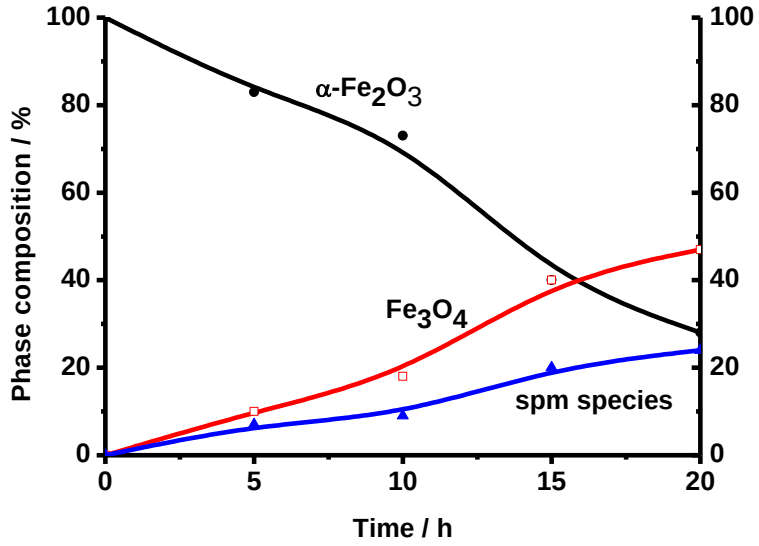

Figure 4-10: The percentage composition versus time when hematite and graphite (3 mol equivalent) mixture was ball milled for different periods whilst the rotational speed and BPR were kept at 20 rpm and at 20:1 respectively.

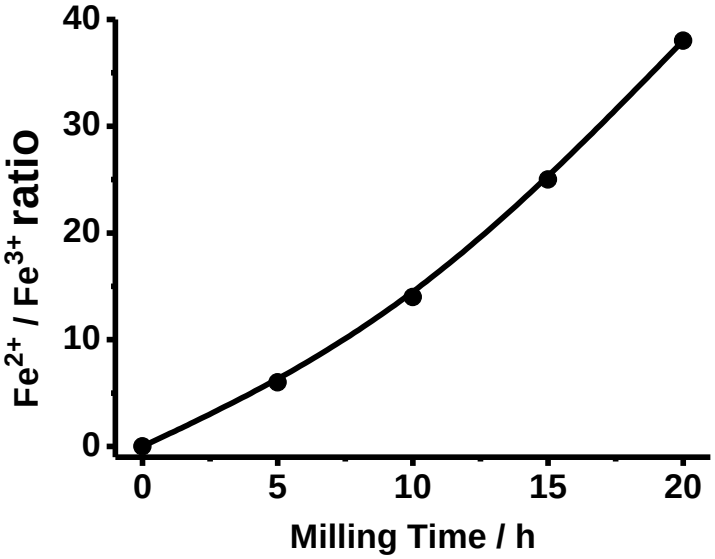

Figure 4-11: Extent of reduction (Fe^{2+}/Fe^{3+}) as a function of rotational period when hematite and graphite (3 mol equivalent) mixture was ball milled for different times whilst the rotational speed and BPR of 20 rpm and 20:1 respectively.

When the BPR was doubled from 10 to 20 rpm, the corresponding Fe^{2+}/Fe^{3+} as determined using MAS was more than squared (see Table 4.3). Thus the dependence of the reduction on BPR was very high, just like the dependence on rotational speed (exponential).

Table 4-3: The effect of BPR variation on phase composition when hematite and graphite (3 mol equivalent) mixture was ball milled for 20h at constant rotational speed (20 rpm).

BPR	α-Fe_2O_3	Fe_3O_4	spm species	Fe^{2+}/Fe^{3+}
10	83 wt.%	11 wt.%	6 wt.%	6
20	22 wt.%	26 wt.%	51 wt.%	38

Further evidence in support of the reduction of hematite to magnetite under reactive milling was obtained using XRD. The x-ray diffractograms are shown in Figure 4-12. The diffractograms show 2θ lines (slightly broader than for un-milled materials) that were unambiguously assigned to hematite, magnetite and graphite phases. Unlike MAS, XRD study was unable to detect spm species (Fe^{2+} and Fe^{3+}) that had much smaller crystallites below its detection limit. The variation in time showed an increment in the magnetite peaks accompanied by recession of hematite and graphite peaks as the milling time was increased. The phenomenon is indicative of the consumption of the starting materials (hematite and graphite) to product (magnetite) as a function of time during the milling process.

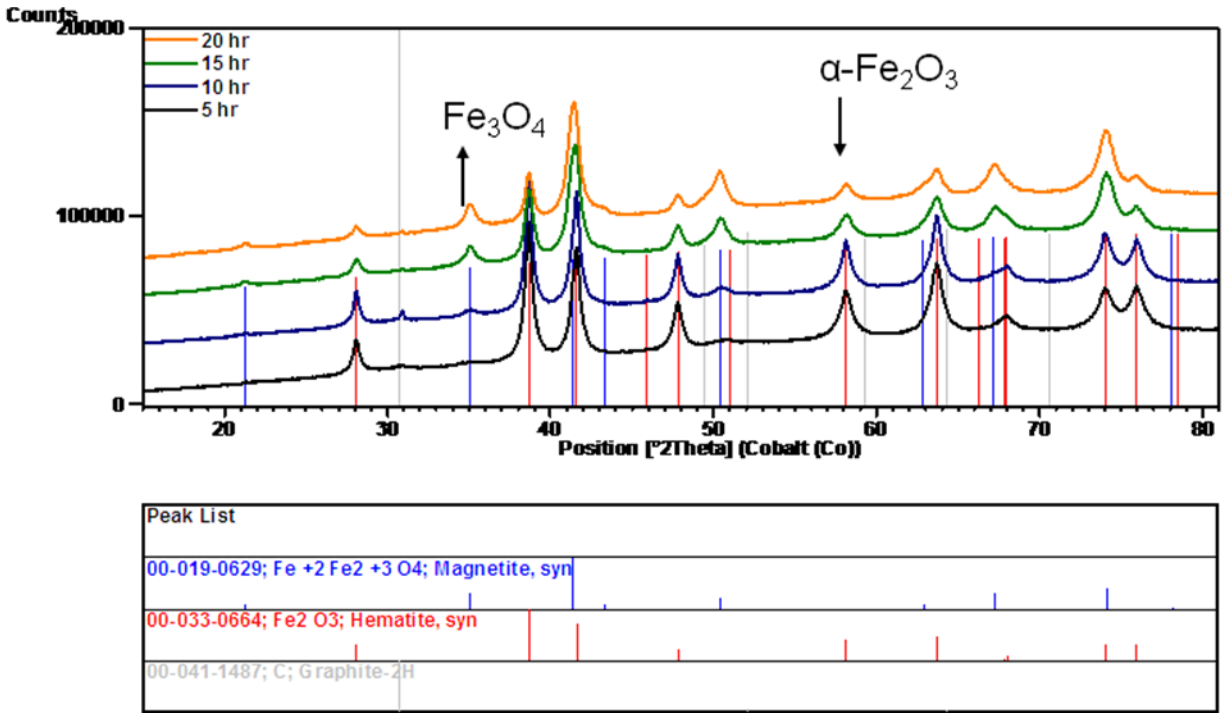

Figure 4-12: X-ray diffractograms obtained when hematite and graphite (3 mol equivalent) mixture was ball milled for different times whilst the rotational speed and BPR were kept constant at 20 rpm and 20:1 respectively

The data analysed gave trends regarding the reduction of hematite to magnetite. However, there was still no proof that during data acquisition, the sample analysed remained true (i.e., it remained un-oxidised in air). To check for possible air oxidation, a sample prepared as usual was exposed to air and MAS spectra recorded at set periods (see Figure 4-13). It was found that the integrity of the sample remained true even for periods up to 10 days. Thus the data obtained in all of the experiments conducted were deemed trustworthy.

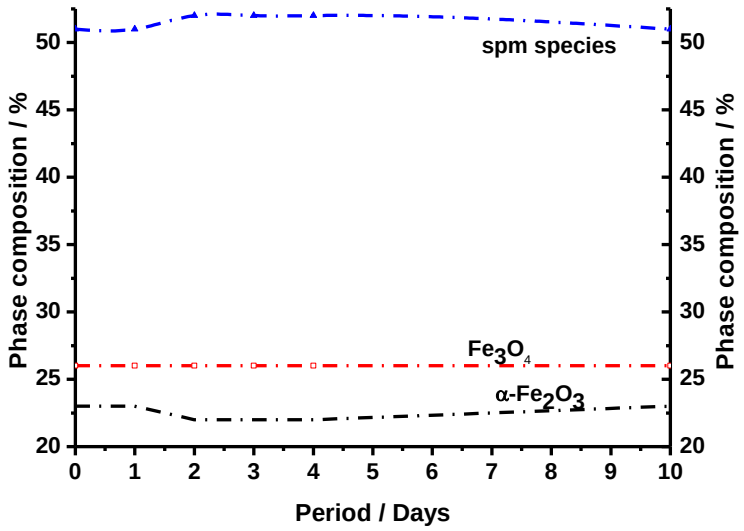

Figure 4-13: The MAS determined phase compositions of a hematite-graphite mixture that was ball milled for 20h at rotational speed of 20:1 and BPR = 20, exposed to atmospheric air for period up to 10 days.

The interaction of hematite and graphite (3:1 mol equivalent), at different milling conditions, lead to the formation of magnetite and unresolved spm Fe^{2+} and or spm Fe^{3+} species depending on the milling conditions. The unresolved spm species were shown to magnetically resolve at low temperatures to either magnetite (major) or hematite (minor). The study shows that by increasing the milling time, the rotational speed and / or the ball to powder ratio, the extent of the transformation of hematite to the above mentioned products increased. It was not possible to reduce beyond magnetite under the experimental conditions (BPR = 20, rotational speed = 20 rpm and milling period = 20h). A further investigation on the reduction behaviour of magnetite was necessary for the elucidation of the reduction behaviour of hematite by graphite.

The reduction of magnetite using graphite was carried out using commercially available magnetite source whose room temperature MAS spectrum is shown in Figure 4-14 and the hyperfine parameters summarised in Table 4-4. The spectrum consisted of two sextets, the first with

parameters, $\delta \sim 0.29$ mm/s, $\Delta E_Q \sim 0.01$ mm/s, Bhf ~ 49.2 T, corresponded to Fe^{3+} on the A site and the second with parameters, $\delta \sim 0.66$ mm/s, $\Delta E_Q \sim 0.01$ mm/s, Bhf ~ 46.0 T, was due to a mixture of Fe^{2+} and Fe^{3+} on the B site. The ratio of Fe^{3+} cations on A-site and B-site as well as Fe^{3+}/Fe^{2+} ratio for a given sample provide an indication of stoichiometry [35]. For commercial magnetite used, the Fe (A-site)/Fe (B-site) ratio was found to be 1:2 while the Fe^{3+}/Fe^{2+} is 2:1 as expected [36].

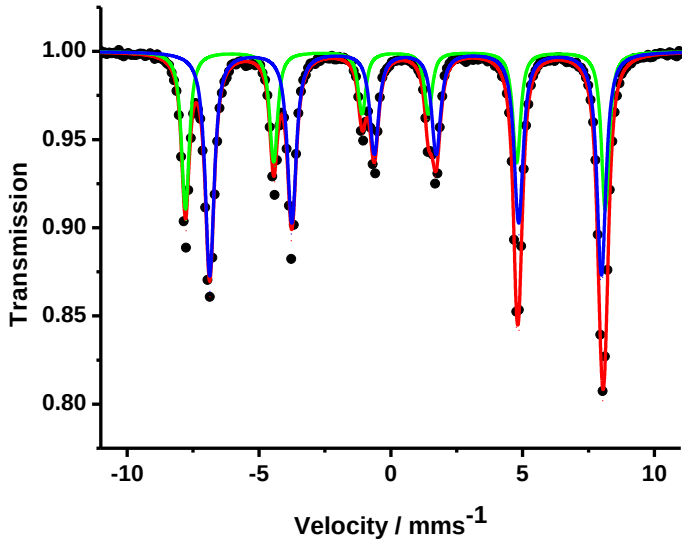

Figure 4-14: Room temperature MAS spectrum of commercial sourced (Sigma-Aldrich) magnetite

Figure 4-15 shows the room temperature MAS spectra of the ball-milled magnetite and graphite mixtures (3: 1 mole equiv) at different ball to powder ratios (BPR) while rotational speed and milling period were kept constant at 400 rpm and 20 hours respectively. The hyperfine parameters for each BPR variation spectrum are summarised in Table 4-4. Figure 4-16 displays the X-ray diffractograms (BPR 20:1 up to 100:1).

Table 4-4: MAS parameters of the ball-milled magnetite and graphite mixtures (3: 1 mole equiv) at different ball to powder ratios (BPR) while rotational speed and milling periods were kept constant at 400 rpm and 20 hours respectively

BPR	MAS parameters			▪% Content	Phases
	# δ / mms^{-1}	# ΔE_Q / mms^{-1}	Φ B_{hf} / T		
0	0.29	0.01	49.2	100	Fe_3O_4
	0.66	0.01	46.0		
20:1	0.29	0.01	48.5	90	Fe_3O_4
	0.61	-0.01	45.1		
	0.35	1.42	-	5	Fe^{3+}
	0.77	1.38	-	5	Fe^{2+}
30:1	0.29	0.02	48.4	42	Fe_3O_4
	0.63	-0.05	45.0		
	0.27	0.38	-	6	Fe^{3+}
	0.89	0.96	-	52	Fe^{2+}
40:1	0.28	0.02	48.4	16	Fe_3O_4
	0.68	-0.05	45.0		
	0.28	0.44	-	11	Fe^{3+}
	0.89	0.92	-	73	Fe^{2+}
50:1	0.28	0.44	-	11	Fe^{3+}
	0.89	0.92	-	89	Fe^{2+}
60:1	0.28	0.44	-	12	Fe^{3+}
	0.89	0.92	-	88	Fe^{2+}

Error: # ± 0.02 mms^{-1}, Φ ± 0.5 T, ▪ ± 1.0%

The spectrum showing the results of ball milling magnetite-graphite mixture at a BPR of 20:1 (Figure 4-4a) was fitted with 2 sextets coexisting with two quadrupole doublets. The two sextets had parameters, $\delta \sim 0.29$ mm/s, $\Delta E_Q \sim 0.01$ mm/s, Bhf ~ 48.5 T, corresponding to Fe^{3+} on the A site and the second with parameters, $\delta \sim 0.61$ mm/s, $\Delta E_Q \sim -0.01$ mm/s, Bhf ~ 45.1 T, that were due to magnetite. The total iron bearing contribution due to this phase was 90 % (relative to the other constituents). Notice that the magnetic hyperfine fields decreased slightly from the typical 49.0 T and 46.0 T for the A and B sites respectively. This observed phenomenon of magnetic hyperfine field reduction could be due to crystallite size reduction and / or defects formation that stem from ball milling effects. The quarupole doublets had parameters, $\delta \sim 0.35$ mm/s, $\Delta E_Q \sim 1.42$ mm/s and δ

~ 0.77 mm/s, ΔE_Q ~ 1.38 mm/s due to Fe^{3+} and Fe^{2+} species respectively. The identity of these species could not be unambiguously assigned using room temperature MAS. Nevertheless, the data implied that the starting material (magnetite) was largely unreduced under the milling conditions employed. The findings were not surprising considering the fact that hematite ball milled under the same conditions, in excess reductant (graphite), only resulted in the formation of magnetite. Thus the energy imparted to the iron-oxide mixture was not sufficient to overcome the activation barrier that could results in the reduction of magnetite. The use of a higher BPR was envisaged as a path towards complete reduction of magnetite. Indeed the X-ray diffractogram (Figure 4-16) displayed 2θ lines that were solely assigned to magnetite. No other crystalline phase was detected.

The spectrum obtained when the magnetite-graphite mixture was subjected to reactive milling at a BPR of 30:1 was also fitted with two sextets and two doublets (Figure 4-15b). The two sextets had parameters synonymous with magnetite and had relative iron content of 42 %. This indeed showed a marked decreased in the relative content of the starting material (magnetite). The relative contents of Fe^{3+} and Fe^{2+} were found to be 6 and 52 % respectively. The higher Fe^{2+} content undeniably signified that magnetite was reduced to a predominantly Fe^{2+} species. Thus the use of higher BPR could promote the reductions of magnetite. The MAS parameters for the Fe^{3+} species, δ ~ 0.27 mm/s, ΔE_Q ~ 0.38 mm/s, were markedly different to the ones obtained when a BPR of 20:1 was used, hinting to the possibility that a different Fe^{2+} species could have been formed. However, without LT-MAS data, the exact identity of the species could not be unambiguously identified. X-ray analysis (Figure 4-16) resulted in diffractogram whose 2θ lines were assigned to magnetite and wüstite. Quantification using XRD was difficult due to overlapping of peaks. Therefore the absolute contribution of the two constituents could not be verified using the two techniques except to say that the bulk of the observed Fe^{2+} species in MAS analysis was due to wüstite.

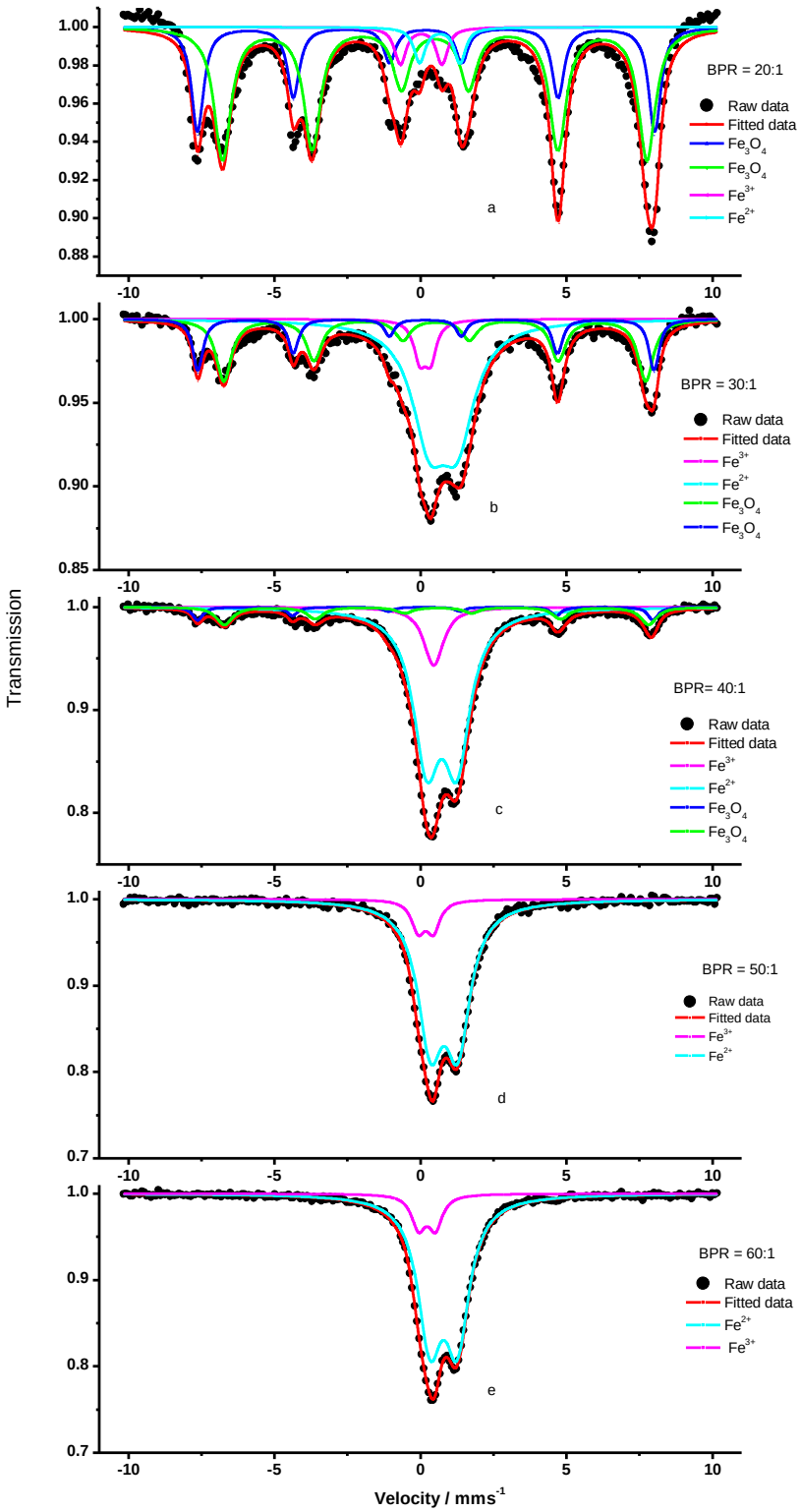

Figure 4-15: Room temperature MAS spectra of the ball-milled magnetite and graphite mixtures (3: 1 mole equiv) at different ball to powder ratios (BPR) while rotational speed and milling periods were kept constant at 400 rpm and 20 hours respectively

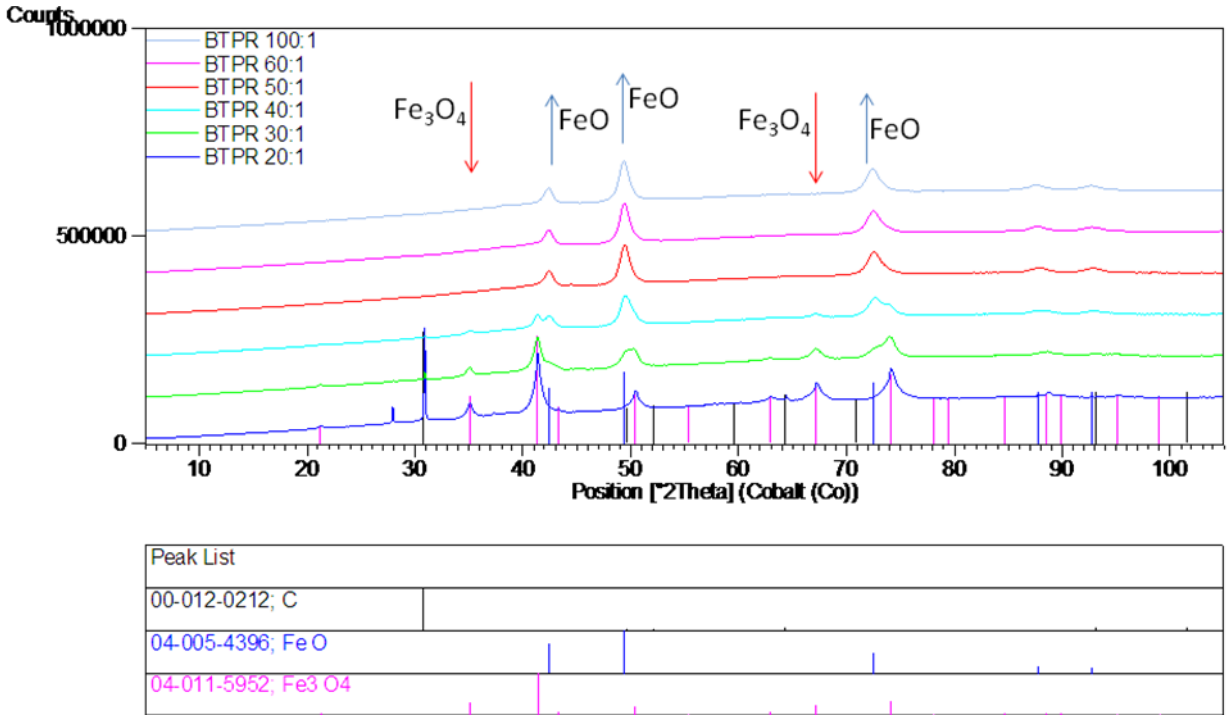

Figure 4-16: X-ray diffractograms of the ball-milled magnetite and graphite mixtures (3: 1 mole equiv) at different ball to powder ratios (BPR) while rotational speed and milling periods were kept constant at 400 rpm and 20 hours respectively.

Wüstite, Fe_xO ($0.89 \leq x \leq 0.98$), has a deficient NaCl structure, space group FM-3m [37]. This structure can be regarded as consisting of two interpenetration fcc cubic structures of Fe^{2+} and O^{-2} where the cubic unit cell contains four units. The unit cell parameter can take values in the range a = 0.428 – 0.431 Å, depending on the vacancy [38]. Wüstite is iron deficient and has an average crystal density of 7.875 $g.cm^{-1}$. The value of the cell parameter of the wüstite crystal lattice varies with x, becoming smaller as x increases. This may cause shifts in the positions of the wüstite peaks on the XRD powder diffractogram and it was the case with the data obtained in this work, i.e., the 2θ values for the three most intense peaks were not exactly 42.12, 49.11 and 87.08 degrees for typical for wüstite. Supposedly, the minor differences observed could have been induced by the milling effect.

The room temperature MAS spectrum of the magnetite-graphite mixture milled when the BPR was set at 40:1 also exhibited two quadrupole doublets and two sextets (Figure 4-15c). The sextets were due to magnetite and its relative content was found to be 16 %. The relative contents of Fe^{3+} and Fe^{2+} were found to be 11 and 72 % respectively indicative of pronounced magnetite The observed Fe^{2+} species is thought to be predominantly wüstite in composition. X-ray study of the same material showed trace contribution of magnetite accompanying wüstite **(Figure 4-16).**

When the BPR was increased further to 50:1, the room temperature MAS spectrum obtained (Figure 4-15) was only fitted with two quadrupole doublets due to Fe^{3+} and Fe^{2+} species contributing about 11 and 89 % respectively (Table 4-4). There was no longer any contribution from the starting material (magnetite). Indeed X-ray probe confirmed the presence of wüstite as the sole crystalline constituent.

The sticky issue that remained unresolved was the exact identity of Fe^{3+} species using MAS, which could have been made easy using LT-MAS probe. It is not uncommon for the MAS spectrum of wüstite to be fitted with a combination of doublets for both Fe^{3+} and Fe^{2+} species, with the majority contributor being the divalent species. McCammon and Price [39] have fitted the spectrum with a superposition of subspectra ascribed to high spin Fe^{2+} high spin Fe^{3+} species. The fitting artefact was thought to reflects the defect structure of wüstite. According, to McCammon, the cubic unit cell contains four units with Fe^{3+} occupying interstitial tetrahedral site surrounded by Fe^{2+} primarily occupying the octahedral sites and octahedral defects. The small contribution from a high spin Fe^{3+} is there to balance the charge loss due to Fe^{2+} vacancies (defects). Hence the observed Fe^{3+} species could have been due to wüstite. Further evidence in support of this theory was the fact that both MAS (Figures 4-15d-e) and XRD (Figure 4-16) analysis for samples subjected to BPR of 60:1 and beyond only resulted in near identical data to that obtained for BPR of 50:1, signifying that nothing else happened as far as reduction was concerned once all the iron oxide was in the form of wüstite. Thus the energy impacted by the balls and bowl on the magnetite-graphite powder was no longer sufficient to reduce FeO any further. In fact even a BPR of 100:1 failed to produce any traces of metallic iron or carbide that would have been a sign that FeO was further reduced.

The reaction of magnetite and graphite (3:1 mol equivalent), at different milling conditions (BPR variations), lead to the formation of Fe^{2+} and or Fe^{3+} species, the former increasing at the expense of magnetite depending on the milling conditions. Magnetite contributions completely disappeared after BPR of 50:1 and beyond as shown by both MAS and XRD. Thus the Fe^{2+} and or Fe^{3+} species remaining beyond BPR of 50:1 were thought to be contributions due to wüstite. Indeed XRD analysis showed that at BPR of 50:1 and beyond, wüstite was the sole crystalline phase detectable. The study shows that by increasing the BPR, whilst keeping the other parameters constant (milling speed and time) magnetite could be selectively reduced to wüstite.

4.3 Characterization of iron oxides by SEM and TEM

4.3.1 Characterization of Hematite and Magnetite by SEM

4.3.1.1 Hematite

SEM images of (a) Fe_2O_3 powder prior to milling at high magnification (1100K X), (b) Fe_2O_3 powder prior to milling at higher magnification (1100K X), (c) after milling for 5h, (d) 10h, (e) 15h, and (f) 20h are shown in Figure Fig 4.14. The crystal habit exhibited was rhombohedral (Fig 4.14a). The displayed macrocrystals were plates of varying lengths that were predominantly hexagonal in shape.

Figure 4-14 shows the SEM micrographs of surface of graphite powder. The multi-layers of graphite sheets were observed and they suggest the existence of sheets of carbon hexagonal nets [28].

When hematite and graphite powders were milled for 5 hours under the experimental conditions stated above (Figure 4.14c), a powder with distinguishable contributors was the product. The larger plates like blocks were iron oxide (Fe_2O_3) while the tiny specs of macrocrystals that adhered to the larger blocks were graphite. The average sizes of the larger hematite plates were estimated to be 100 - 500 nm. When the milling period was sequentially increased to 10h, 15h and 20h, significant changes on the powder mixture were observed, prominent being the texture; such that the particle textures appeared rougher than those of the Fe_2O_3 powder prior to milling.

The once well-defined hematite particles gradually took ill-defined shapes and these particles became smaller in size as the milling period was increased. This was as a result of the milling action that induced reaction between the two powders (hematite and graphite) to form magnetite (a reduction product). It is envisaged that the magnetite product is incorporated in the mushy powder that is predominantly composed of graphite.

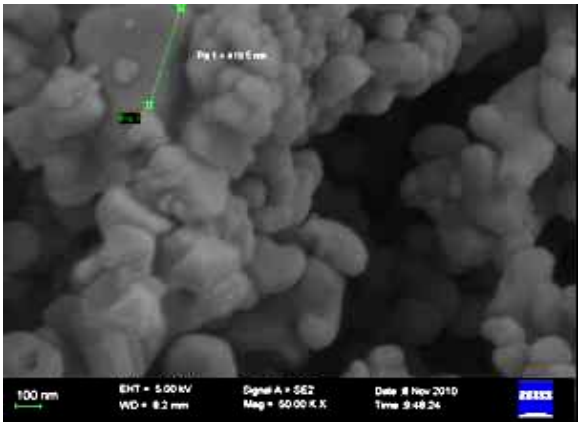

(a)

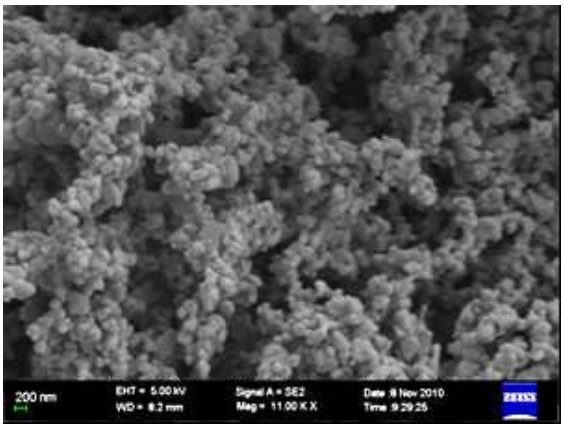

(b)

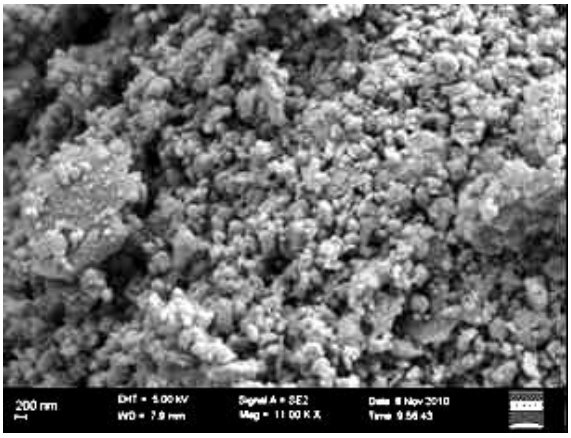

(c)

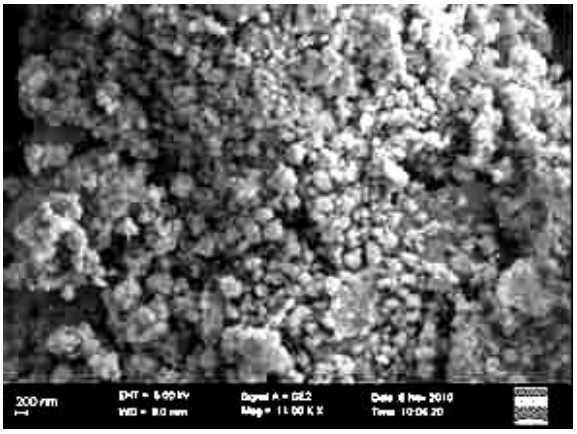

(d)

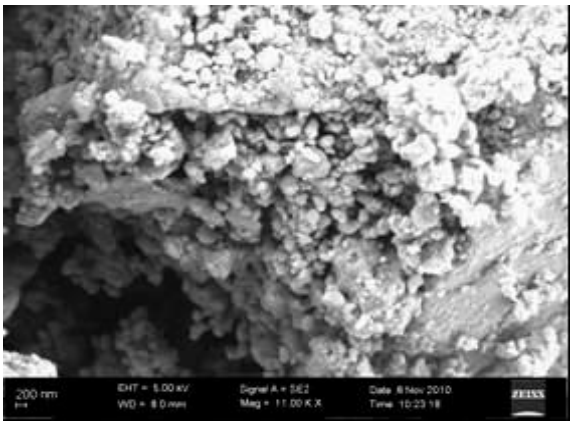

(e)

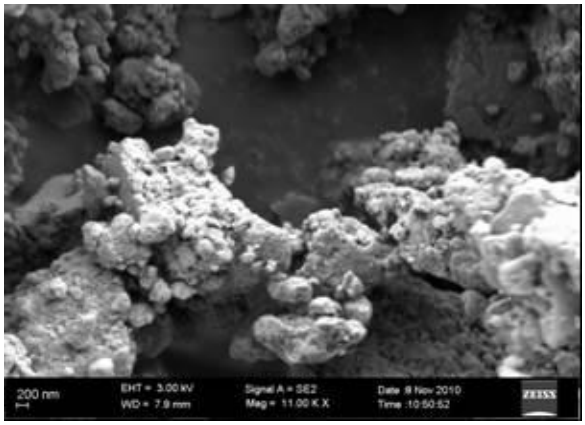

(f)

Figure 4-15: SEM images of (a) Fe_2O_3 powder prior to milling at Higher magnification (50 00K X), (b) Fe_2O_3 powder prior to milling at Low magnification (11 00K X), (c) after milling for 5h, (d) 10h, (e) 15h, and (f) 20h

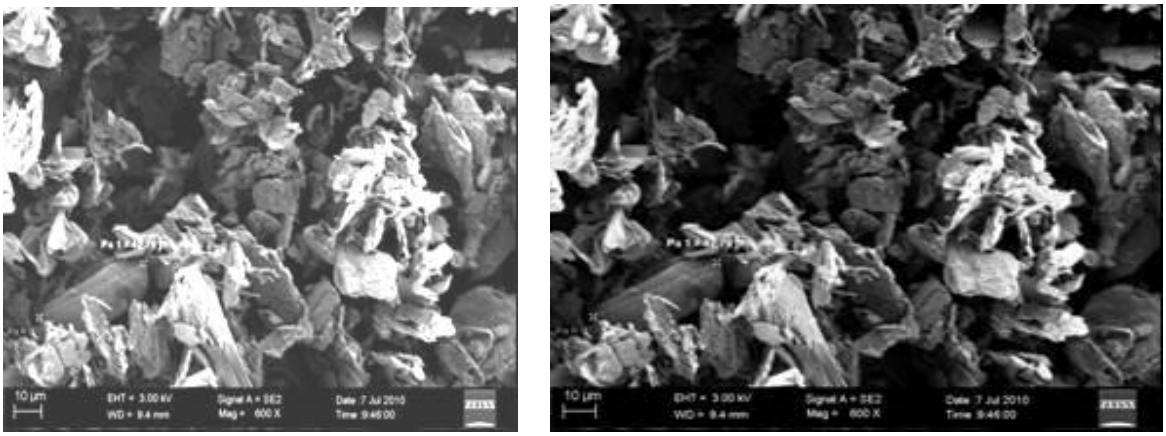

Figure 4-16: SEM images of graphite at lower magnification (600X)

A Representative Backscatter Electron (BSE) image of pure Fe_2O_3 is shown in Figure 4.16. The dark area represents the background and the lighter, irregular shapes represent individual particles of hematite (Figure 4-16a). Upon expansion (Figure 4-16b, at higher magnification , 200X) it became apparent that the particles contained a multitude of crystallites of varying sizes.

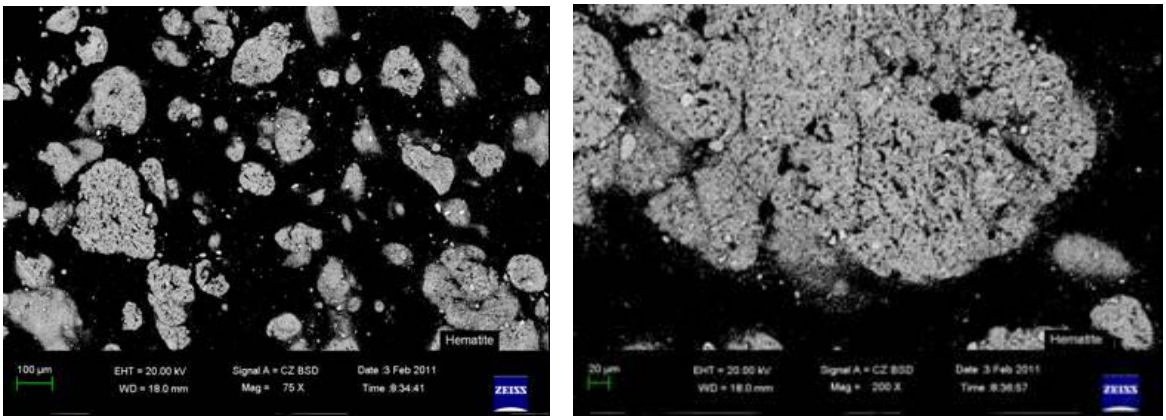

(a) (b)

Figure 4-17: BSE images of hematite at different magnifications a (75X) and b (200X)

Figure 4-17 shows the BSE images of hematite-graphite mixture milled for 20h (when the BPR was kept constant at 20:1 and rotational speed = 400 rpm). The image shows that the once larger particles of hematite have shrunk significantly in size after the milling period. Figure 4-17a Also shown is the emergence of plate-like materials, which were thought to be the product of the reduction process, magnetite. Indeed the pure magnetite BSE images (shown in Figure 4-18), does display plate-like granules, confirming the inference above. Just like hematite, each magnetite particle seemed to be composed of many tightly held microcrystallites **(Figure 4-17b)**.

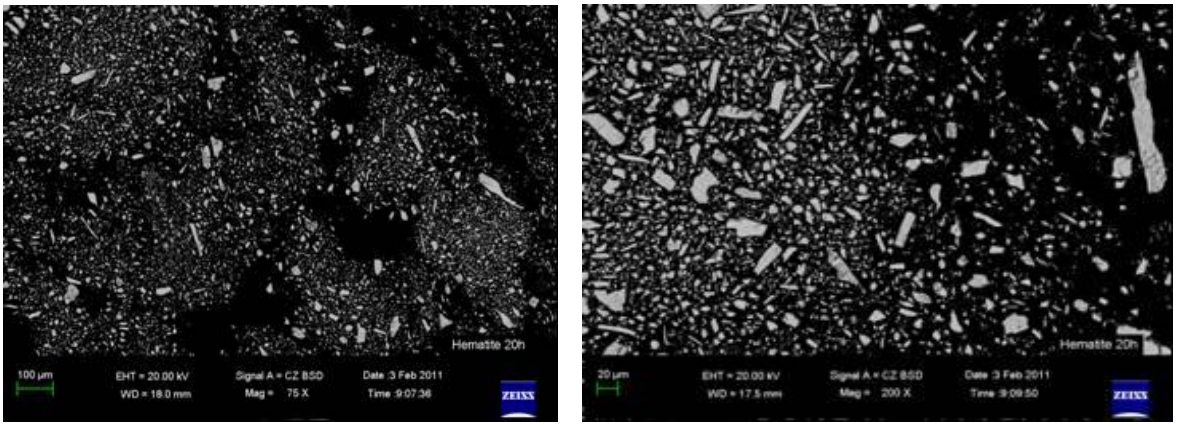

(a) (b)

Figure 4-18: BSE images of hematite-graphite mixture milled for 20h (BPR = 20:1, 400 rpm) at different magnifications a (75X) and b (200X)

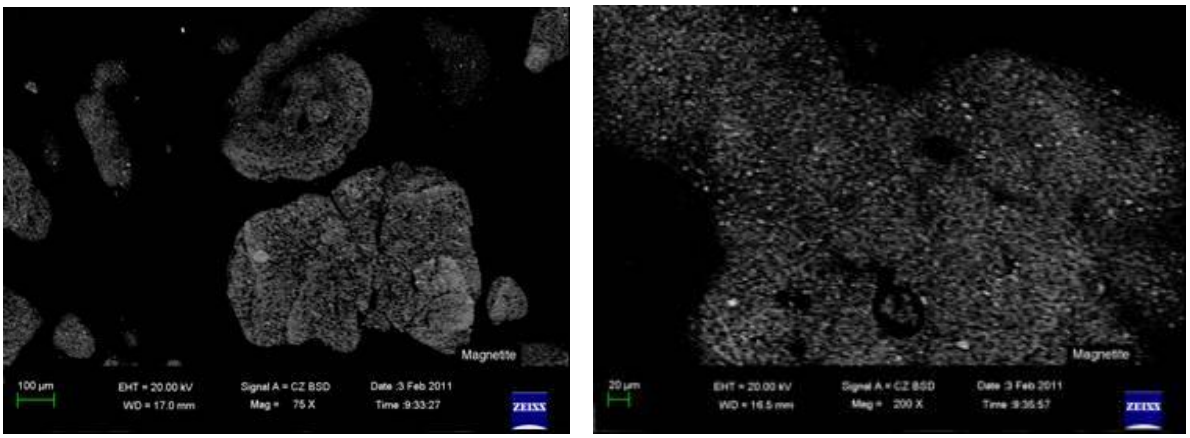

(5a) (5b)

Figure 4-19: BSE images of pure magnetite at different magnifications 5a (75X) and 5b (200X)

Elemental analysis and quantification were performed in order to confirm if not verify the elemental composition of the three samples of interest, hematite, magnetite and the magnetite-graphite mixture that was milled for 20h (BPR = 20:1, 400 rpm). For each sample studies, Electron Diffraction X-ray (EDX) spectra from 3 representative areas were obtained and the quantification results averaged to get the mean value for each element identified see spectra's in Figures 4-20 – 4-22. The EDX results displaying the detected elemental compositions and respective area ratios are summarised in Tables 4-4, 4-5 and 4-6. The calculations to confirm elemental composition are reported in Annexure 1. EDX study indicated that the three samples studied; pure hematite,

hematite-graphite and pure magnetite were composed chiefly of iron, in addition to carbon, oxygen constituents. The unexpected impurities; chlorine, gold and palladium were present in very low quantities as can be seen in the Tables 4-4 to 4-6, they were mostly likely introduced during the sample preparation for SEM imaging.

Table 4-4 shows the EDX data for the pure hematite. Using the data, it was shown that the predicted iron and oxygen contents were 70.9 and 29.1 % respectively **(see Annexure 1)**. These values are closed to the expected iron and oxygen content values of 69.9 % and 30.1 % from the stoichiometric calculations. The data thus confirmed that the EDX generated data was sufficient to quantify the individual constituents of the iron oxide mixture.

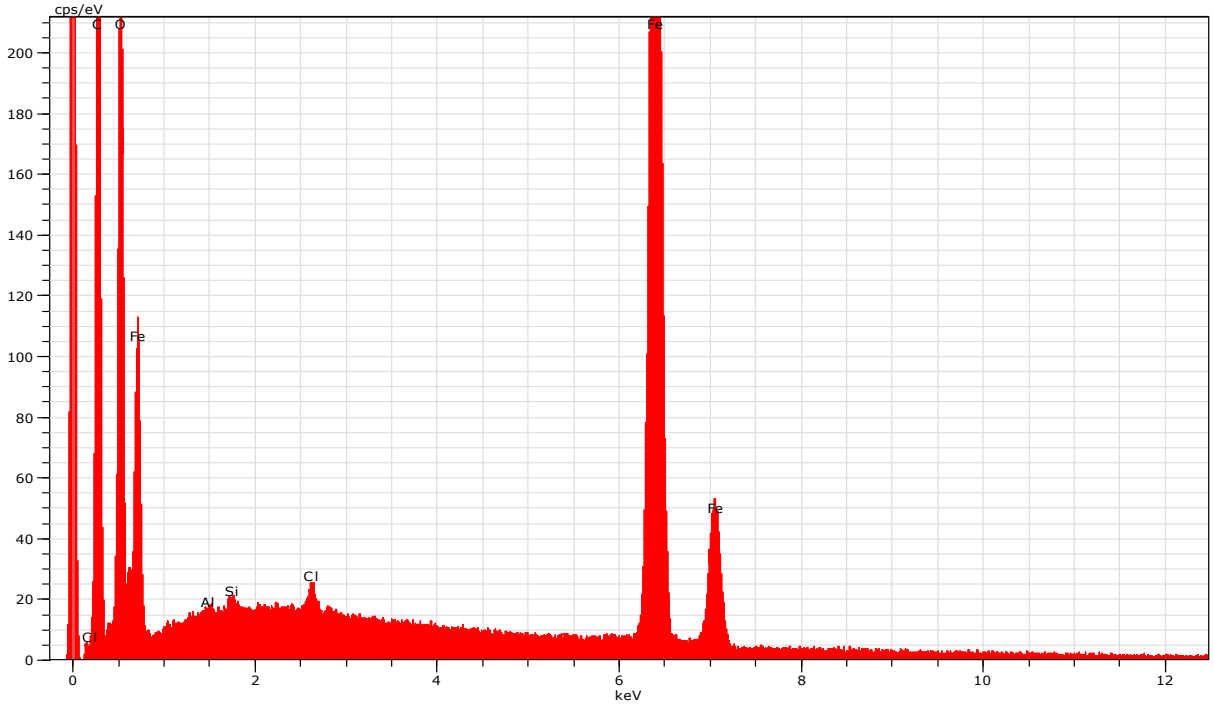

Figure 4-20a: EDX spectra of Hematite

Table 4-4: EDX generated data when pure Fe_2O_3 (constituents in mass percent %) was studied

Spectrum	C	O	Cl	Pd	Au	Fe
Spectrum 1	11.33	26.96	0.29	0.26	1.46	56.24
Spectrum 2	11.79	22.68	0.33	0.29	1.89	57.81
Spectrum 3	12.35	21.68	0.33	0.35	2.31	59.42
Mean	**11.82**	**23.77**	**0.32**	**0.30**	**1.88**	**57.82**

Figure 4-20 exhibit the EDX spectra of hematite-graphite mixture milled for 20h (BPR = 20:1, 400 rpm). The EDX data obtained is shown in Table 4-5. The calculations showed that the iron and oxygen percentage contents were 66.7 and 33.3% respectively, suggesting that the mixture contend reduction materials beyond magnetite. Indeed the EDX data for pure magnetite are summarized in Table 4.6, from which it was deduced that the iron and oxygen percentage contents were 73.0 and 27.0 % respectively; values that are close to the expected 72.4 and 32.6 for iron and oxygen respectively using stoichiometry.

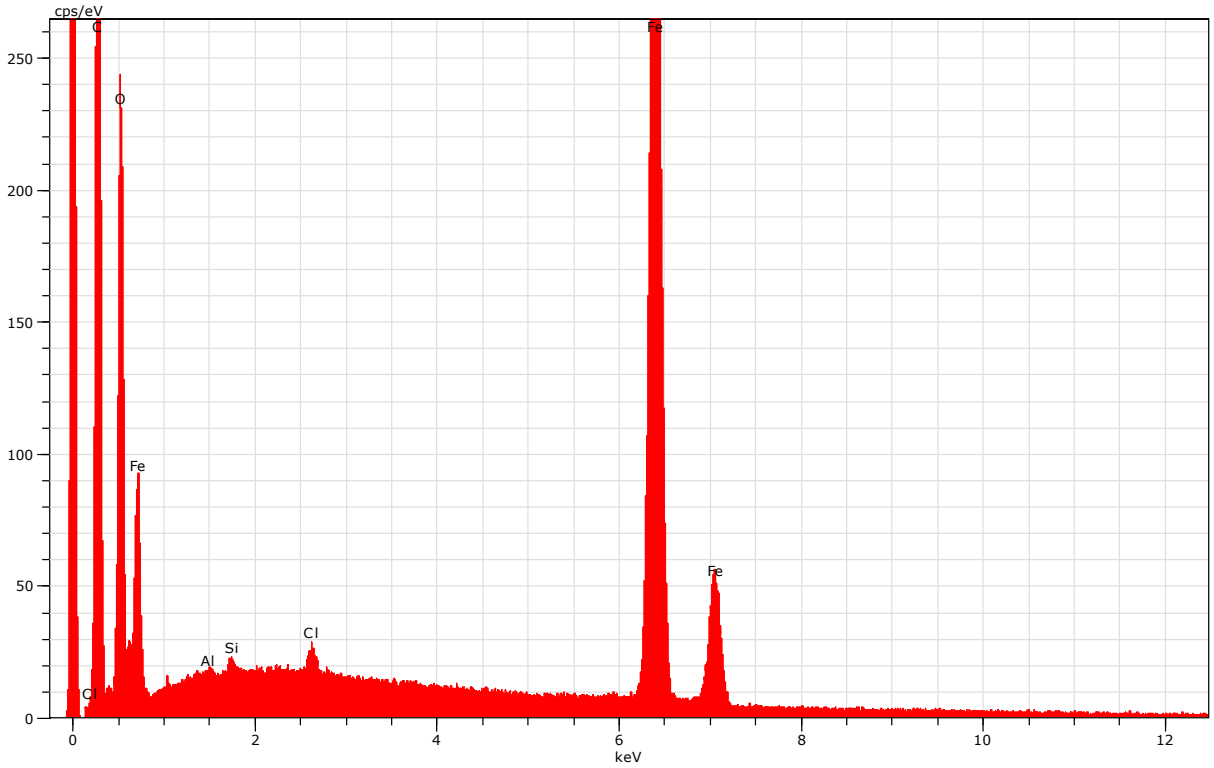

Figure 4-21: EDX spectra of Hematite milled for 20hours

Table 4-5: EDX generated data for Fe_2O_3–graphite mixture milled for 20h (where the constituents are recorded in mass percent %) was studied

Spectrum	C	O	Cl	Pd	Au	Fe
Spectrum 1	3.10	29.50	0.03	0.23	1.89	64.41
Spectrum 2	2.91	28.26	0.05	0.28	2.05	65.22
Spectrum 3	3.92	34.32	0.07	0.22	1.42	55.13
Mean	**3.31**	**30.70**	**0.05**	**0.24**	**1.78**	**61.59**

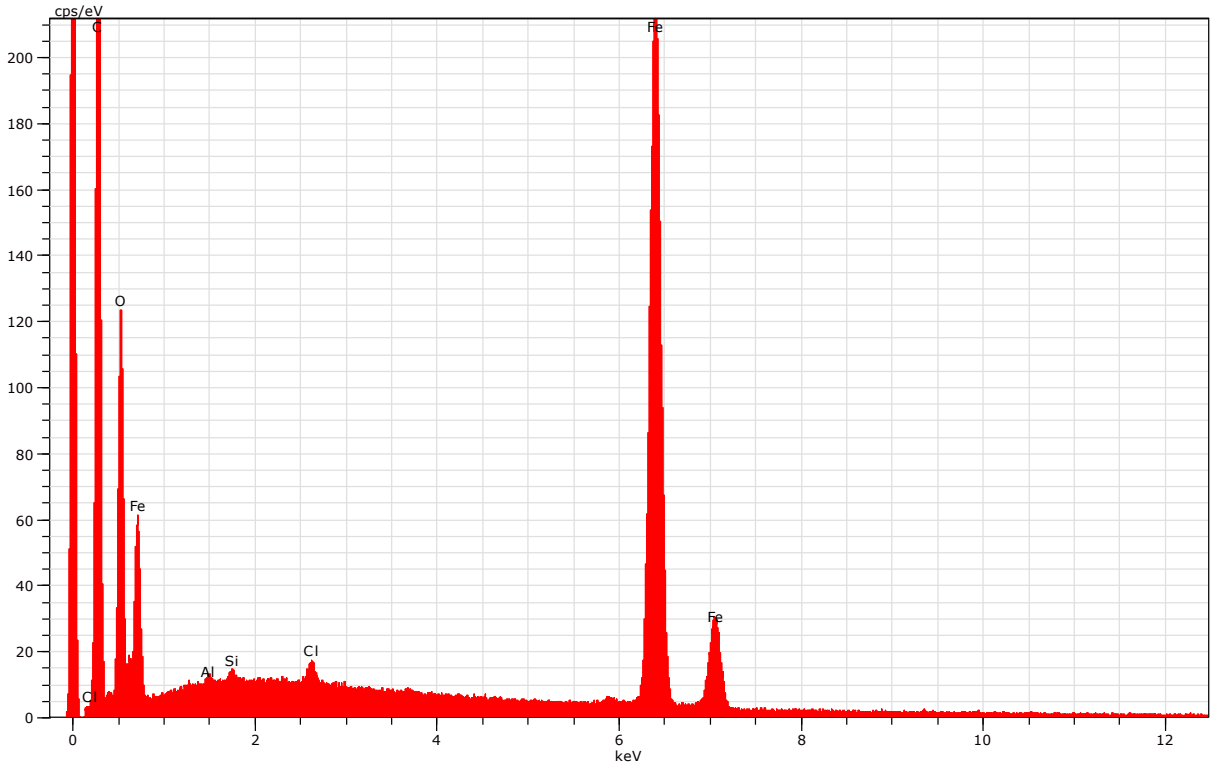

Figure 4-22: EDX spectra of Magnetite

Table 4-6: EDX generated data for Fe_3O_4 (whose constituents in mass percent %) that was studied

Spectrum	C	O	Cl	Pd	Au	Fe
Spectrum 1	16.38	20.15	0.34	0.31	2.27	52.92
Spectrum 2	16.96	18.56	0.36	0.35	2.57	54.50
Spectrum 3	17.85	20.05	0.35	0.33	2.36	51.06
Mean	**17.06**	**19.58**	**0.35**	**0.33**	**2.40**	**52.82**

4.3.1.2 Magnetite

SEM images of (a) Fe_3O_4 powder prior to milling at high magnification (5000K X) (b) Fe_3O_4 powder prior to milling at low magnification (11 00K X), (c) after milling at 20:1 BPR (d) 30:1 BPR (e) 40:1 BPR (f) 50:1 BPR (g) 60:1 BPR (h) 100:1 BPR are shown in Figure 4.20.

Pure magnetite sample exhibited well-defined octahedral particles of different sizes **(see Figure 4-20b)**. When magnetite and graphite powders were milled at different BPR under the experimental conditions stated above, progressively, smaller particles seemed to have been forming. In additions, the particles observed seemed to have been deformed (and as such lack the well defined shape originally observed for the unmilled material). The deformation was more pronounced at higher BPR.

When EDX mapping was used, followed by calculations of the iron-oxide ratios, it was determined that the major constituent when BPRs were 20:1 and 30:1was magnetite. Meanwhile, for the BPRs of 50:1, 60:1 and 100:1 the predominant phase using the deduced data was found to be wustite **(see Annexure 1)**. Indeed the use of XRD also confirmed the above mentioned phases at the specified BPRs. The study also revealed that the sample obtained when the BPR of 40:1 was used, had both magnetite and wustite in coexistence. The SEM study indicated that the surfaces of the sample were very compact and boundaries of different phases were not easily observed.

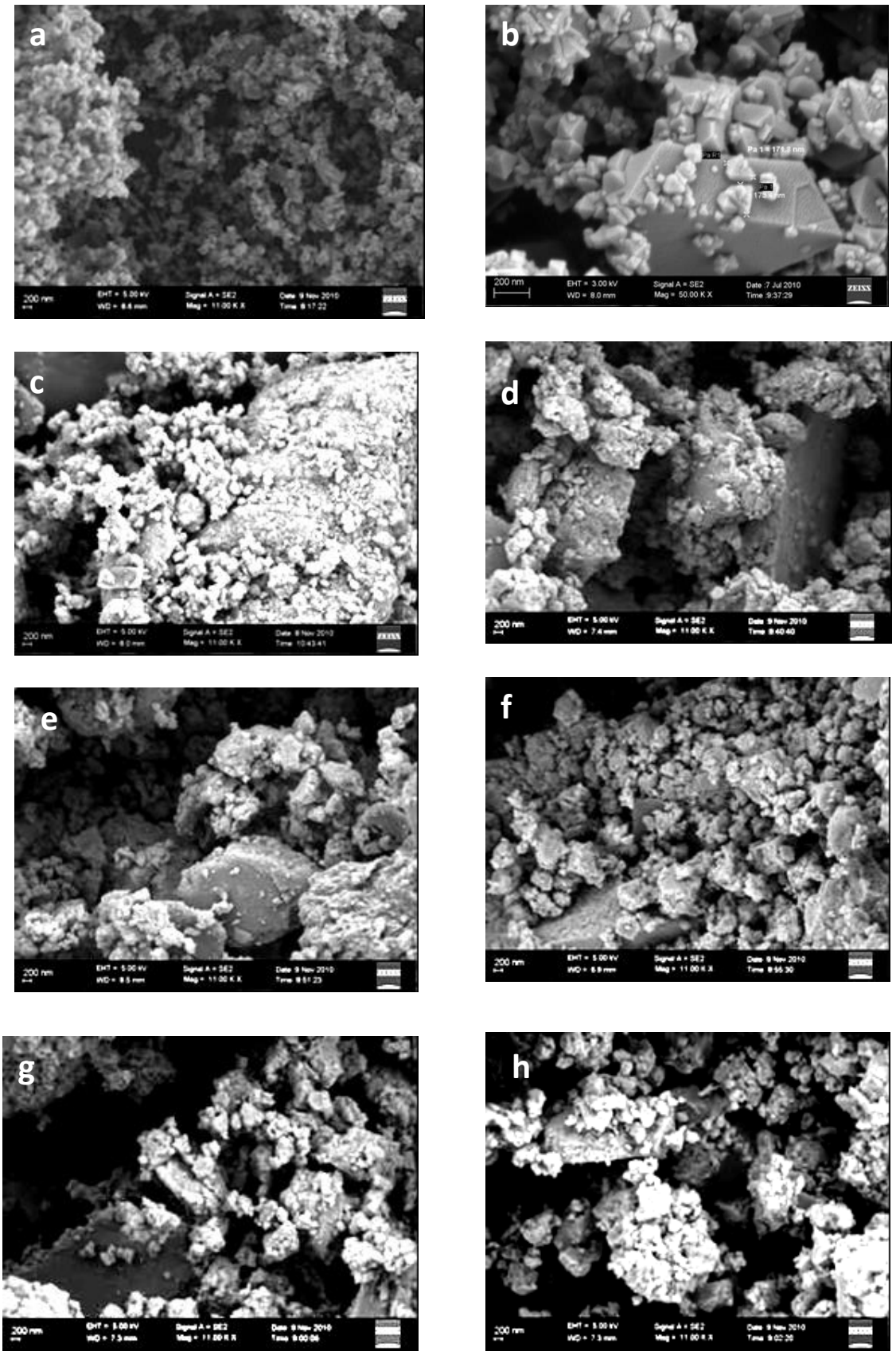

Figure 4-23: SEM images of (a) Fe_3O_4 powder prior to milling at high magnification (50 00K X) (b) Fe_3O_4 powder prior to milling at low magnification (11 00K X) (c) 20:1 BPR (d) 30:1 BPR (e) 40:1 BPR (f) 50:1 BPR (g) 60:1 BPR (h) 100:1 BPR .

4.3.2 Characterization of Hematite and Magnetite by TEM

4.3.2.1 Hematite

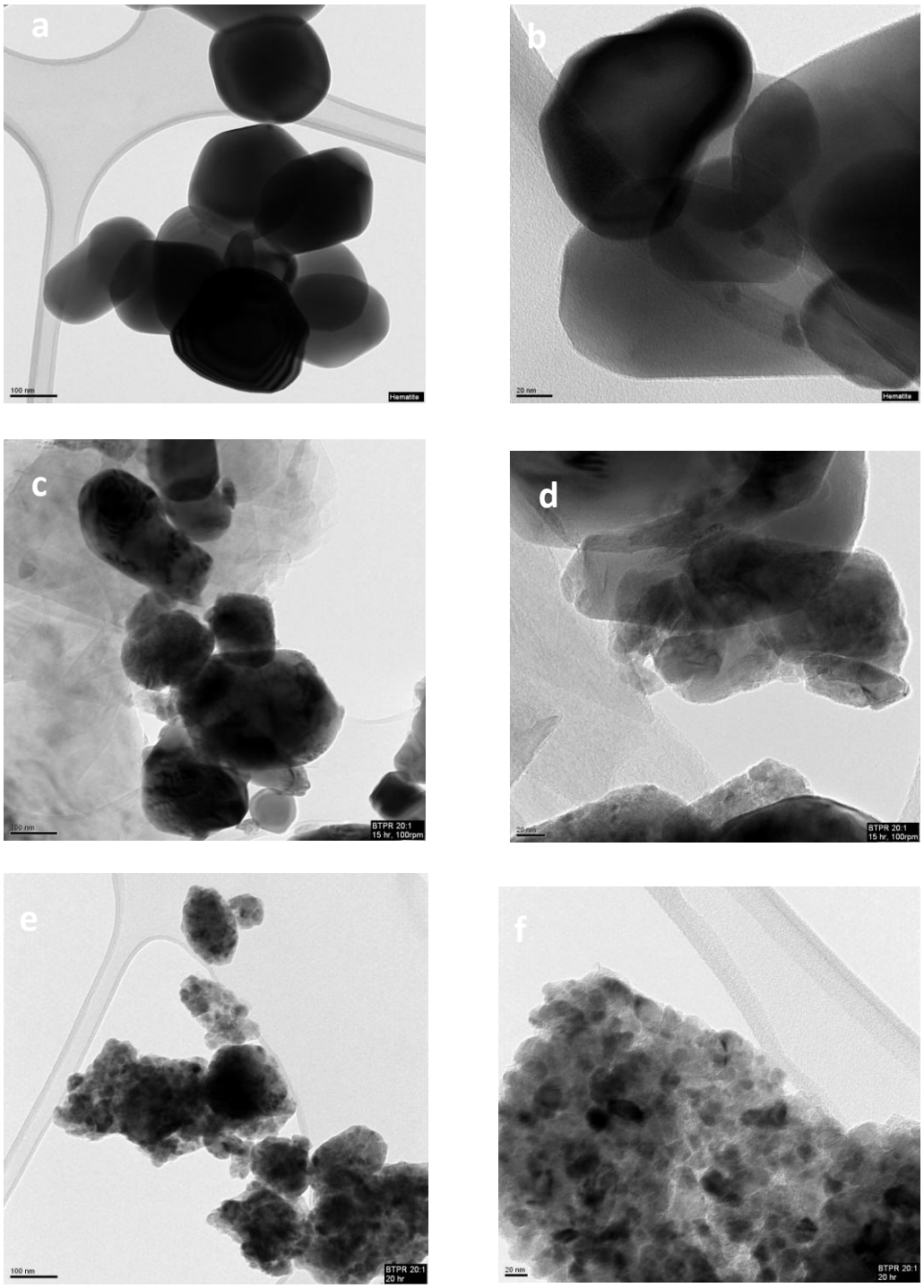

Figure 4-24: Low magnification transmission electron micrograph of pure Hematite (a) at 100nm, (b) at 20 nm magnifications, (c) TEM image (100nm) for hematite-graphite (3 mol equivalent) subjected to ball milling conditions for 15h and at higher magnification (d) (10 nm). (e) TEM image (100 nm) for hematite-graphite (3 mol equivalent) subjected to ball milling conditions for 20h and at higher magnification (10 nm).

Figure 4-24a shows the low magnification transmission electron micrograph of pure hematite. The image exhibits several well defined hematite particles, each composed of several crystallites of the iron oxide phase (see the higher resolution on **Figure 4-24b**). The shapes of the particles are different but the predominant shape seemed to have been hexagon. What was also observed was that the particle size (measured by taking the longest distance from one end of the crystal to another was less than 150 nm (on average it was about 110 nm).

Figure 4-24c shows the low magnification transmission electron micrograph of hematite-graphite mixture that was milled for 15h at BPR of 20:1, 400rpm. The hematite particles were still observed (dark particles) but they seemed to have been fractured. Focusing on one of the particles at higher magnification (Figure 4.24d), it can be seen that the particle is composed of agglomerated sub particles. The fracture points are probably the reaction fronts where magnetite was formed from the reduction of hematite using graphite. The lighter and much smaller particles sprinkled all over the sample are probably the graphite particles. Due to particle fragmentation, it became more difficult to approximate the particle size.

Figure 4-24e shows the low magnification transmission electron micrograph of hematite-graphite mixture that was milled for 20h at BPR of 20:1, 400rpm. The degree of hematite particle degradation/fragmentation increased, as evidenced by the presence of smaller particles. Focusing on one of this particles at higher magnification **(Figure 4.24f)**, the image depicts an infusion of micro crystals in close proximity. There are more lightly shaded particles than before suggesting that the degree of magnetite formation was higher (a fact proven by other techniques).

4.3.2.2 Magnetite

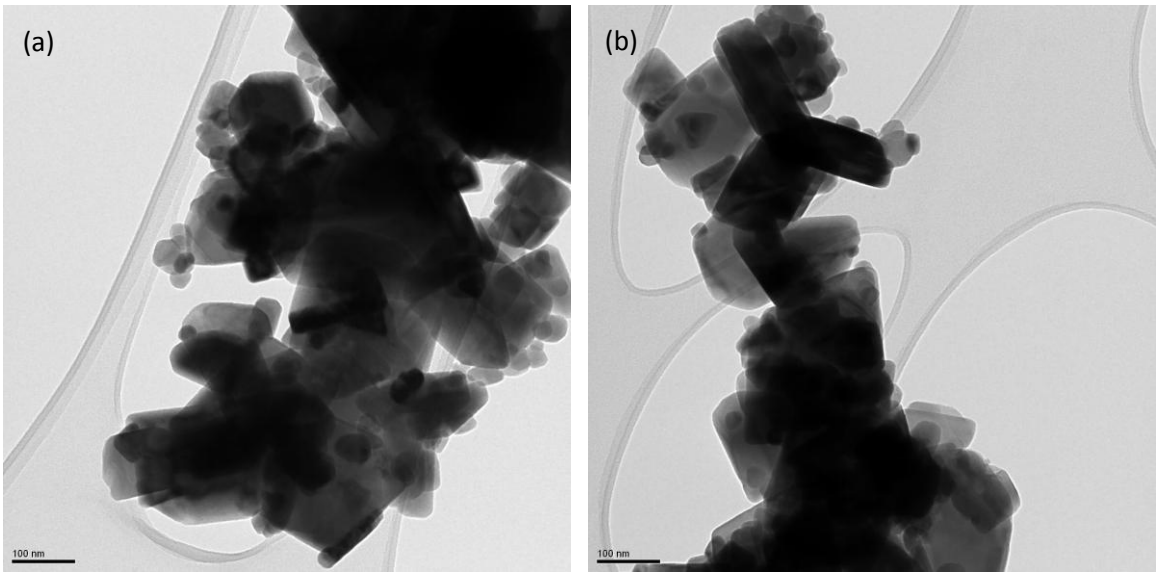

Figure 4-25a shows the low magnification transmission electron micrograph of pure magnetite. The image exhibits several well defined magnetite particles (Figure 4.25b). The shapes of the particles are different but the predominant shape seemed to have been octahedral.

Figure 4-25c shows the low magnification transmission electron micrograph of magnetite-graphite mixture that was milled for 15h at BPR of 50:1, 400rpm. The magnetite particles are completely fractured to fine particles. Focusing on one of the particles at higher magnification **(Figure 4-25d),** it can be seen that the particle is composed of clustered particles that are crystalline. The fracture points are probably the reaction fronts where wustite was formed as a result of the reduction of magnetite using graphite. The observed particle fragmentation made it difficult to approximate individual particle size.

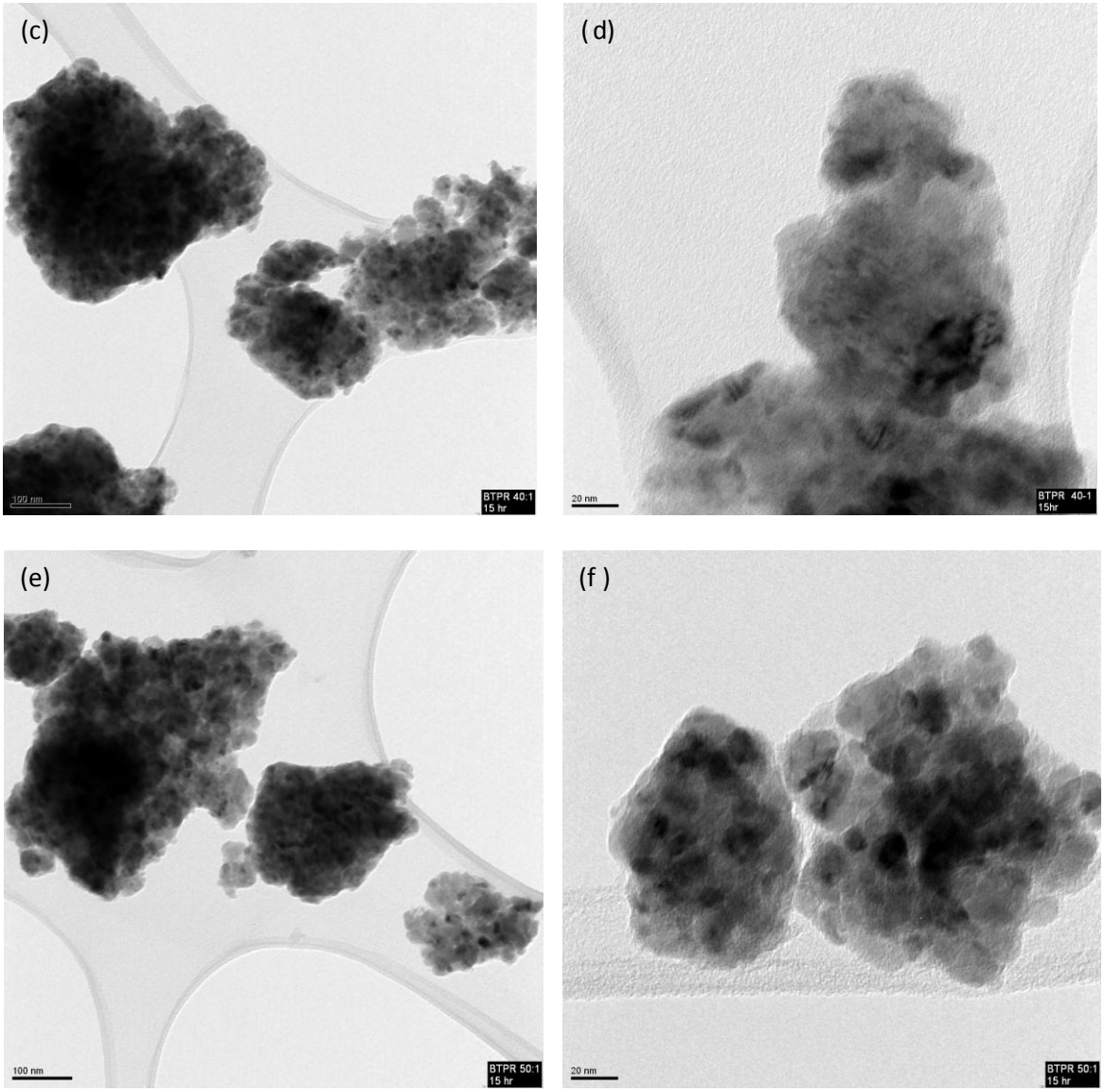

Figure 4-25: Low magnification transmission electron micrograph of pure Magnetite (a) at 100nm, (b) at 100 nm magnifications, (c) TEM image (100nm) for magnetite-graphite (3 mol equivalent) subjected to ball milling conditions for 15h and at higher magnification (d) (10 nm). (e) TEM image (100nm) for magnetite-graphite (3 mol equivalent) subjected to ball milling conditions for 15h and at higher magnification (10 nm).

CHAPTER FIVE

5 CONCLUSIONS AND RECOMMENDATIONS

5.1 Conclusions

The objectives of this investigation were to investigate the solid state reaction of hematite and magnetite with graphite using mechanical alloying. This was to check whether magnetite and/or wustite form as intermediates during the reduction reaction as reported by different authors.

The following conclusion were drawn from this research project:

- MAS showed that the reactive milling of α- Fe_2O_3 and C resulted in reduction to Fe_3O_4 , FeO and or cementite depending on the milling conditions etc Time, milling speed and BPR variation which influenced the reduction. The study shows that by increasing the milling time, the rotational speed and / or the ball to powder ratio, the extent of the conversion of hematite to its reduction products increased, the findings were in agreement with thermodynamics. Further investigations are required for the elucidation of the reduction mechanism.

- XRD study investigations even though were unable to detect spm species (Fe^{2+} and Fe^{3+}) which has smaller crystallites below detection limits, the variation in time showed an increment in the magnetite peaks accompanied by recession of hematite and graphite peaks as the milling time was increased which collaborated to the MAS observation. XRD was also in agreement with the data obtained from MAS that showed that the main constituent was magnetite.

- The reaction of magnetite and graphite (3:1 mol equivalent), at different milling conditions (BPR variations), lead to the formation of Fe^{2+} and or Fe^{3+} species, the former increasing at the expense of magnetite depending on the milling conditions. Magnetite contributions completely disappeared after BPR of 50:1 and beyond as shown by both MAS and XRD. Thus the Fe^{2+} and or Fe^{3+} species remaining beyond BPR of 50:1 were thought to be contributions due to wüstite. Indeed XRD analysis showed that at BPR of 50:1 and beyond, wüstite was the sole crystalline phase detectable. The study shows that by increasing the

BPR, whilst keeping the other parameters constant (milling speed and time) magnetite could be selectively reduced to wüstite.

- Characterization of the HRSEM images Fe_2O_3 using Scanning electron mi[cr]oscopy [pr]ior to milling at different times showed significant changes while the milling period was increased, HRSEM images showed that the once well defined hematite particles took an ill-defined shapes and also became smaller in size, which was a results of the milling action that induced reaction between the two powders to form magnetite. The BSE images and EDX spectra at different milling time**s** also confirmed formation of magnetite, where darker areas are Fe_3O_4 and EDX elemental analysis and quantification confirmed the elemental composition of starting materials (Fe_2O_3) and final product (Fe_3O_4)
- Characterization of Fe_3O_4 using SEMprior to and after milling at different BPR showed significant changes while the milling period was increased. HRSEM images showed mushy and ill - defined shapes features after milling. The BSE and EDX studies at different milling times also confirmed formation of partial FeO, and EDX elemental analysis and quantification confirmed the elemental composition of starting materials (Fe_3O_4) And the formed product FeO.
- Characterization using TEM showed that both Fe_2O_3 and Fe_3O_4 at different BPR and times showed significant changes to both particles and confirmed that their respective transformation (reduction) was accompanied by crystallite size reductions as well.

5.2 Recommendations for future work

- To attempt to reduce the hematite fully to α-Fe by increasing the energy required of the reaction mixture.

6 REFERENCES

1. Calka A., Kaczmareck W.A., Ninham B.W. and Radlinski A.P., *Mater. Sci. Eng., A.*, 1991, **134**, 1346.
2. Prakash S., *J.S. Afr. Inst. Min. Metall*., 1996, **96**, 3
3. Khaki J.V., Kashiwaya Y., Ishii K. and Suzuki H., *ISIJ Int*., 2002, **42**, 22.
4. Gavrilenko I. S., Mordyuk B.N., Nadutov V.M and Prokopenko G.I*., Ultrason.,* 2004, **42**, 47.
5. Nowosielski R. and Pilarczyk W., *J. Mater. Process. Technol*., 2005, **162-163**, 373.
6. Grenèche J.M., Hervieuc M., Mercier A.M. and Randrianantoandro N., *Mater. Lett*., 2001, **47**,150.
7. Khaki J.V., Aboutalebi M.R. and Raygan S., *Miner. Process. Extr. Metall. Rev*., 2004, **25**, 29.
8. Cótica L.F., Da Cunha J.B.M., Luciano A., Paesano Jr A. and Santos I. A., *J. Magn. Mater*., 2004, **281**, 227.
9. Suryanarayana C., *Mechanical Alloying and Milling*, Marcel Dekker, New York, 2004.
10. Benjamin J.S. and Gilman P.S., *Mechanical Alloying*, Annual Review, New York, 1983.
11. Berbenni V., Chapman P.G. and Welham N.J., *Carbon,* 2002, **40,** 2307.
12. Calka A., Guo Z.P., Huang Z.G., Liu H.K. and Wexler D., *J. Alloys Compd*, 2007, **427**, 94.
13. Aboutalebi M.R., Khaki J.V., Raygan S., *Miner. Process. Extr. Metall. Rev*., 2004, **25**, 29-47.
14. Uehara, Y., "Structural changes of iron oxides by ball-milling in different media," *Bull. Chem.Soc.* Japan, 1975,**48**,pp. 3383 – 3384
15. Lecaer, G., and Matteazzi, P., "Reduction of hematite with carbon by room temperature ball milling", *Mater. Sci. Eng., A.,* 1991, A149*,* pp*.135*– 142.
16. Kaczmarek, W.A., Ninham, B.W., and Onyskiewicz, I., "Structural and magnetic characteristics of novel method of Fe_2O_3 double-right-arrow Fe_3O_4 reduction by magneto mechanical activation," IEE transaction on magnetics, 1994, **30**, pp. 4725– 4727.

17. Campbell, S.J., Kaczmarek, W.A., and Wang, G.M., “Mechananochemical transformation of hematite to magnetite,” *Nanostructured Materials*, **6**, pp. 735– 738.

18. Linderoth, S., Morups, S., and Jiang, J.Z., “Reversible α-Fe_2O_3 to Fe_3O_4 transformation during ball milling,” *Mater. Sci.Forum,* 1997, **235 – 238**, pp.205 -210.

19. Jovalekic, C., Karanovic L.J., Mitric, M., Poleti, D., Skala, D., and Zdujic, M., “Mechanochemical treatment of α-Fe_2O_3 powder in air atmosphere,” *Mater. Sci. Eng., A.,* 1998, **A245**, pp. 109 **–**117.

20. Jovalekic, C., Karanovic L.J., Mitric, M., and Zdujic, M., “The ball milling induced transformation of α-Fe_2O_3 powder in air and oxygen atmosphere,” *Mater. Sci. Eng., A.,* 1999, **A262**, pp. 204 **–**213.

21. Lecaer, G., and Matteazzi, P., “Mechanochemical reduction of hematite by room temperature ball milling”, *Mater. Sci. Eng., A.,* 1991, **68***,* pp.177– 180.

22. Tokumitsu, K., “Reduction of metal oxides by mechanical alloying method,” *Solid state Ionics,* 1997, 101 – 103, pp. 25– 31.

23. Balaz, P., Extractive Metallurgy of Activated Minerals, Amsterdam, 2000, Elsevier.

24. Boldyrev, V. V., and Tkacova, K., “Mechanochemistry of solids: Past, present and prospects,” *Journal of materials synthesis and processing*, 2000, **8**, pp. 121– 132.

25. McCormick P. G., and Schaffer, G. B., “Reduction of metal oxides by mechanical alloying,” *Applied Physic Letters*, 1989, **55**, pp.45-46.

26. Suryanarayana, C., “Mechanical Alloying and Milling,” Progress in Materials Science, 2001, **46**, pp. 1- 184.

27. Ishii, K., Kashiwaya, Y., Suzuki, H., Vahdati Khaki, J., “ Intensive improvement of reduction rate of hematite- graphite mixture by mechanical milling,” ISIJ International, 2002, **36**,pp.1309- 1315.

28. Cornell R.M. and Schwertmann U., The Iron Oxides: structure, properties, reactions, occurrences and uses, 2nd Ed. Wiley-VCH, Weinheim, 2006.

29. Kuzmann E., Nagy S. and Vértes A., Pure Appl. Chem. **75** (2003) 801 – 858.

30. Solheid P. A., The IRM Quaterley, **8** (1998).

31. Schünemann V. and Winkler H., Rep. Prog. Phys. **63** (2000) 263.

32. Belozerski G., Mössbauer effect and studies of surface layers”, web edition.

33. Sinnecker S., Slep L. D., Bill E. and Neese F., Inorg. Chem. **44** (2005) 2245.

34. Pankhurst Q.A., Hyperfine Inter., **90** (1994) 201 -214.

35. U. Schwertmann and R.M Cornell. "*Iron Oxides in the Laboratory".***2nd** ed.**,** Wiley-VCH publishers, New York, 2000.

36. Murad E. and Johns*ton J. H., Mössbauer Spectroscopy* Appl**i**ed to Inorganic Chemistry, eds. G. Long, and F. Grandjean*, Vol 2, Plenum Press, New York***, 19**89

37. A. Gualtieri and P. Venturelli, *Am. Mineral.*, 1999, **84,** 895

38. *J.L. Hazemann, J.F. Berar and* **A.** Manceau, *Mater. Sci*., 1991, **Forum 79**, 821.

39. A. McCammon and D.C. Price, *Phys. Chem. Minerals*, 1985, **11**, 250.

7 Annexure 1

Calculations for the iron-oxide content using EDX data (see Tables 4.4 – 4.6) for three samples, pure hematite, pure magnetite and hematite-graphite mixture milled for 20 hours (BPR = 20:1, 400 rpm):

Hematite (Fe_2O_3)

O : Fe

The total mass of the two constituents (oxygen and iron): 23.77 + 57.82 = 81.59

Binary % values

% O = 23.77/81.59 X 100

= 29.1 %

%Fe = 70.9 %

But in actual Fe_2O_3:

Fe_2O_3 = Mr 159.7 g/mol

Fe = Mr 55.847 g/mol

O = Mr 15.9994 g/mol

%Fe = 2x Mr_{Fe} / Mr_{Fe2O3} X 100

= 69.9 %

%O = 30.1%

Hematite (Fe_2O_3) milled 20h

O : Fe

The total mass of the two constituents (oxygen and iron) = 30.70 + 61.59 = 92.29

Binary % values

% O = 30.70/92.29 X 100

= 33.26 %

% Fe = 66.74 %

But in actual Fe_2O_3:

Fe_2O_3 = Mr 159.7 g/mol

Fe = Mr 55.847 g/mol

O = Mr 15.9994 g/mol

%Fe = 2x Mr_{Fe} / Mr_{Fe2O3} X 100

= 69.9 %

%O = 30.1%

Magnetite (Fe_3O_4)

O : Fe

The total mass of the two constituents (oxygen and iron): 19.58 + 52.82 = 72.4

Binary % values

% O = 19.58/72.4 X 100

= 27.0 %

% Fe = 73.0 %

But in actual Fe_2O_3:

Fe_3O_4 = Mr 231.539 g/mol

Fe = Mr 55.847 g/mol

O = Mr 15.9994 g/mol

%Fe = 3x Mr_{Fe} / Mr_{Fe2O3} X 100

= 72.4 %

%O = 27.6%